ELSEVIER

Contents lists available at ScienceDirect

Biosensors and Bioelectronics

journal homepage: http://www.elsevier.com/locate/bios





Electrically conducting polymers for bio-interfacing electronics: From neural and cardiac interfaces to bone and artificial tissue biomaterials

Seunghyeon Lee a,b, Busra Ozlu b, Taesik Eom b, David C. Martin c,**, Bong Sup Shim b, Taesik Eom b, David C. Martin c,**

- a Department of Chemical Engineering, Inha University 100 Inharo, Incheon, 22212, South Korea
- ^b Program in Biomedical Science & Engineering, Inha University 100 Inharo, Incheon, 22212, South Korea
- ^c Department of Materials Science and Engineering, University of Delaware, Newark, DE 19716, USA

ARTICLE INFO

Keywords: Conductive polymers Neural interfaces Tissue regeneration Bioelectronics Implantable electronics

ABSTRACT

Conductive polymers (CPs) are gaining considerable attention as materials for implantable bioelectronics due to their unique features such as electronic-ionic hybrid conductivity, mechanical softness, ease of chemical modification, as well as moderate biocompatibility. CPs have been utilized for a wide range of applications including neural engineering, regenerative medicine, multi-functional sensors and actuators. This review focuses on CP materials design for use in bio-interfacing electronics including composites, conductive hydrogels, and electrochemical deposition. We start by elaborating on the fundamental materials characteristics of CPs, including bioelectrochemical charge-transfer mechanisms, and contrast them with naturally derived CPs. We then present recent critical examples of the bioelectronic and biomedical applications of CPs, including neural recording and stimulation, tissue regeneration, stretchable electronics, and mechanical actuation. We conclude with a perspective of the current material challenges of CPs in bio-interfacing electronics.

1. Introduction

Electrically conductive polymers (CPs) have become attractive for actively interfacing living systems with abiotic devices, including implantable bionics and bioelectronics (Larsson et al., 2013; Liu et al., 2020; Löffler et al., 2015). The unique features of CPs such as electronic-ionic hybrid conductivity, mechanical softness, permeable porosity, and versatile chemical modification make them favored for a wide range of biomedical device applications including biosensors, chemical sensors, drug delivery systems, artificial muscles, and neural interfaces (Ding et al., 2019; Ding and Lisak, 2019; Inal et al., 2018; Joon et al., 2019; Lisak et al., 2018; Long et al., 2011).

While implantable brain-machine interfaces were initially developed for patients with traumatic injuries (Klein et al., 2012; Schoenen et al., 2005; Wong et al., 1994), therapeutic neuro-stimulation techniques also have been used for treating neurological diseases such as epilepsy (Theodore and Fisher, 2004), chronic pain (Baughman and Shacklette, 1991; Schläpfer and Kayser, 2014), Parkinson's disease (Krack et al., 2003), Lou Gehrig's disease, and depression (Schläpfer and Kayser, 2014). Recently, therapeutic electroceuticals have been further investigated to treat various dysfunctions by identifying the signaling

network and delivering neural impulses to the brain area associated with the diseases. Functionally seamless and chronically compatible interfaces between bio-tissues and electronics are crucial to developing these technologies. However, conventional inorganic materials such as metals and ceramics have limitations due to significant property mismatches, which eventually leads to mechanical trauma and chronic inflammation at the interface (Baughman and Shacklette, 1991). As alternative material solutions, CPs and their composites have the advantages of relatively low modulus; good electrochemical performance; high surface area; in situ production and functional modification with proteins and bioactive molecules; and the capability to load drugs and biomolecules. Several studies have also shown that these CPs can be used in regenerative medicine as electrically-active tissue scaffolds which regulate cellular behavior including adhesion, growth (Collazos-Castro et al., 2010; Quigley et al., 2009; Wong et al., 1994), migration (Gumus et al., 2010), and the regeneration of damaged tissue (Guex et al., 2017; Kenry and Liu, 2018; Kotwal and Schmidt, 2001; Mihic

In this review, we have highlighted recent advances in the design of CPs and their recent application in neural recording and stimulation, artificial sensors and actuators, as well as tissue regeneration. Moreover,

E-mail addresses: milty@udel.edu (D.C. Martin), bshim@inha.ac.kr (B.S. Shim).

^{*} Corresponding author. Department of Chemical Engineering, Inha University 100 Inharo, Incheon, 22212, South Korea.

^{**} Corresponding author.

we also discuss the natural conductive polymers melanin and polydopamines promising candidates for implantable bioelectronics.

2. Electrically conducting polymers

A conjugated molecular backbone, which consists of chains of alternating single and double bonds, is an essential structure for the polymers to have electrical conductivity. This conjugated structure facilitates electron delocalization by overlapping of p-orbitals. The conductivity of CPs can be significantly modulated with various types of dopants (Bredas and Street, 1985; Green et al., 2010; Sinha et al., 2009) (Fig. 1). Electrically active, doped CPs can form a variety of complex microstructures ranging from fully amorphous to moderately crystalline due to relatively weakly bonded polymer chains with conformational freedom. Furthermore, the size and the connectivity of macroscopic domains, the morphological properties, crystallinity, and orientation of the crystallite affect the charge-carrier mobility intensively (Chang et al., 2004; Kline et al., 2005; Sirringhaus et al., 1999). Synthetic CPs such as polyaniline (PANI), polythiophene (PT), polypyrrole (PPy), poly (3,4-ethylenedioxy-thiophene) (PEDOT) have been frequently used in the biomedical electronics applications. Their chemical details and physicochemical properties are well documented in several recent excellent review articles: for general CPs (Kaur et al., 2015), for PPy (Ateh et al., 2006), for PANI (Zare et al., 2019), and for PEDOT (Strakosas et al., 2016). Briefly, the electronic and ionic hybrid conductivities of CPs are sensitively affected by 1) molecular weights of conjugated backbones, 2) π - π stacked crystalline domain sizes, 3) interactions with p-type doping counterions, 4) protonic transporting pathways, 5) electron transfer through hydrogen bonds, and 6) molecular ordering (Fig. 1).

Several synthetically prepared CPs are promising for bio-interfaces, biosensors, and bio-medicines. CPs have many advantages based on their large effective surface area for exchanging charges, high non-faradaic charge transfer, and overall low impedances while forming electrochemical circuits with biotic interfaces (Martin and Malliaras, 2016). Biocompatibility and biosafety are also critical parameters for selecting CPs, not just electrochemical performances. PANI has moderate biocompatibility, excellent stability, and low cytotoxicity (Bidez et al., 2006; Humpolicek et al., 2012; Liu et al., 2010), whereas oligomers of PANI show cytotoxicity depending on the number of repeating

units, time, and concentration (Zhang et al., 2012). PPv is an excellent electrical conductor with biocompatible, cytocompatible and has demonstrated to supporting cell adhesion, growth, regeneration of axons, and modulating cellular response (Garner et al., 1999; Rivers et al., 2002; bib_Williams_and_Doherty_1994; Williams and Doherty, 1994; Zhao et al., 2020) However, the mechanical stiffness of PPy is not matched to biological tissues (Qi et al., 2017; Zhou et al., 2018). PEDOT has been extensively studied, which is the most successful derivative of polythiophene in the field of biomedical engineering (Kaur et al., 2015; Martin et al., 2010; Peramo et al., 2008) because of its high electrical conductivity and superior chemical stability (particularly when compared to PPy), along with biocompatibility (Green and Abidian, 2015; Kaur et al., 2015). Despite the dramatic advancement made in synthetic CPs, there are still limitations such as poor long-term stability, insufficient mechanical matches with biotic tissues, and chronic biocompatibility (Kaur et al., 2015).

Alternatively, natural CPs are emerging as active bioelectronic materials including melanin-like materials, which possess high electrical conductivity (Baraldi et al., 1979; McGinness et al., 1974; McGinness, 1972; Osak et al., 1989; Powell and Rosenberg, 1970), biocompatibility (Bettinger et al., 2009), and anti-inflammatory properties (Eom et al., 2017). Recently, T. Eom et al. fabricated free-standing natural melanin composite films with electrical conductivity of 1.17 S/cm (Eom et al., 2019). However, biointerfacing electronics application examples using melanin-like materials are still limited at this moment.

3. Bioelectronic applications of conducting polymers

3.1. Neural recordings and stimulations

Early progress in the use of CPs in biomedical applications focused on the development of neural electrodes, which serve as a crucial electronic interface to the biological systems (Guimard et al., 2007; Patil and Thakor, 2016). This requires an optimized interface between the electrode and neural tissue as well as efficient signal transfer between the cells and the electrode (Guimard et al., 2007). There are several parameters that need to be considered while designing neural electrodes, such as providing large charge storage capacity (CSC), charge injection limit (CIL), low impedance, and high signal to noise ratio (SNR). Electrochemical impedance spectroscopy (EIS) also provide information of

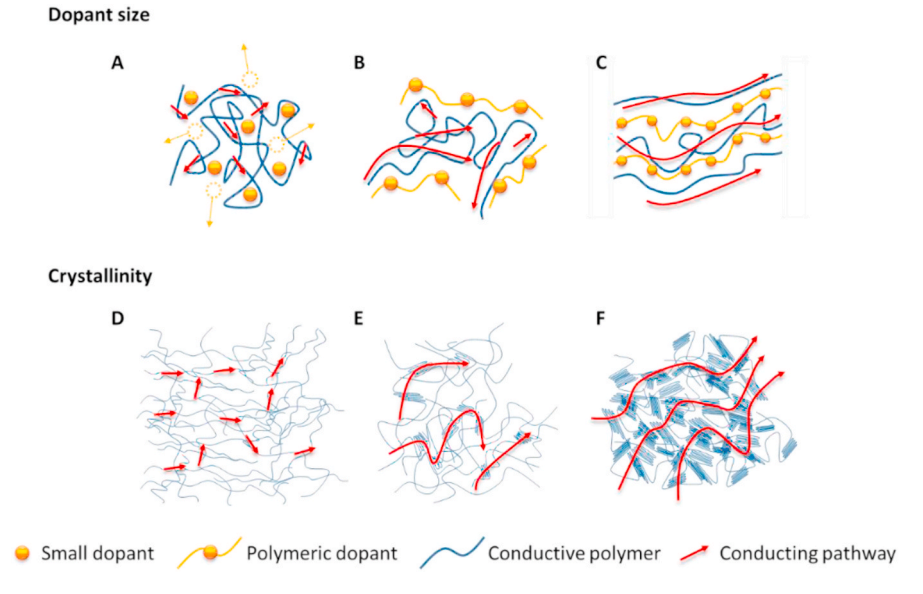


Fig. 1. Schematics of molecular structures of CPs of showing (A–C) interactions with counterions or dopants and (D–E) delocalized charge pathways along with different sizes of crystal domains. (A) Small molecules, (B) oligomeric, and (C) polymeric dopants. (D) Amorphous, (E) low crystalline, and (F) high crystalline conjugated domains of the conductive structures.

CPs at the bio-interfaces such as reactions and kinetics at the electrode-media interfaces, dielectric and transport properties of materials (Ciucci, 2019; Lasia, 2002; Lvovich, 2012; Macdonald, 2006). These fundamental theories and experimental techniques are already well documented, and the readers can find excellent reviews (Cogan, 2008; Green and Abidian, 2015; Woeppel et al., 2017). EIS spectra can be interpreted in terms of equivalent circuit (EEC) models that help explain the predominant mode of charge transport in the system. One common model is the Randles circuit, which gives values of parameters such as general impedance, double layer capacitance, solution resistance, polarization resistance and Warburg impedance. The components depict a coupling between the charge transport of the reactants and the products. The ability of EIS to analyze both dynamic and spatial elements of interfacial kinetics makes it an important tool to be used in vivo clinical applications (Kleber et al., 2017; Lvovich, 2012; Opie et al., 2016). As the CV technique provides specific information on the CSC and durability of the electrode, the combination of EIS with CV provides a detailed understanding of the properties of conductive polymers (Ates, 2011). The CIL is determined by the maximum amount of charges delivered within the range where a pseudocapacitive reversible reaction occurs. In general, the CIL is determined by the maximum cathodal potential excursion (E_{mc}), which is the boundary where the voltage transients do not cause a Faradaic reaction, especially water electrolysis. To find CIL, biphasic stimulations are generally used for applying current. As excess charges can trigger electrochemical reactions cathodic and anodic charges should be balanced not to damage tissue or electrode (Cogan, 2008). This process that resembles the impulse conduction mechanism of nerve with Na⁺ and K⁺ movement mitigates the damage on tissue caused by the unbalancing charge effectively (Fig. 2). While the method to stimulate the nerve follows the internal signaling mechanism of nerve, CPs can further offer the potential to mimic the function of nerve with its selective ion transporting ability (Akieh-Pirkanniemi et al., 2016; Arroyo et al., 2019).

CPs in the neural interfaces can increase the effective charge exchanging surface area while maintaining a small geometric electrode size (Green and Abidian, 2015). Other criteria, such as biocompatibility and long-term durability, can also be met by designing CP hybrid neural electrodes. Various ions, proteins, and cells interact with an electrode implanted in the body, which results in an extraordinarily dynamic and rigid condition for the neural electrode. Thus, CPs placed at the neural electrode interface can play a specific role in maintaining stable and biocompatible to minimize the acute and chronic inflammation, which eventually leads to a decrease and an ultimate loss in signal transduction (Kim et al., 2017; Meijs et al., 2016).

Providing high effective surface area and promoting facile ion exchange between recording sites and surrounding tissues make CPs promising candidates as interfacing electrodes (Patil and Thakor, 2016). The recent achievements and the current trends in CP research were described in the following parts (Fig. 3 and Table 1).

For neural recording and stimulation, the superior electrochemical performances presented by low electrochemical impedance, a large CSC, and a high CIL are the essential factors. On top of this, long-term stability

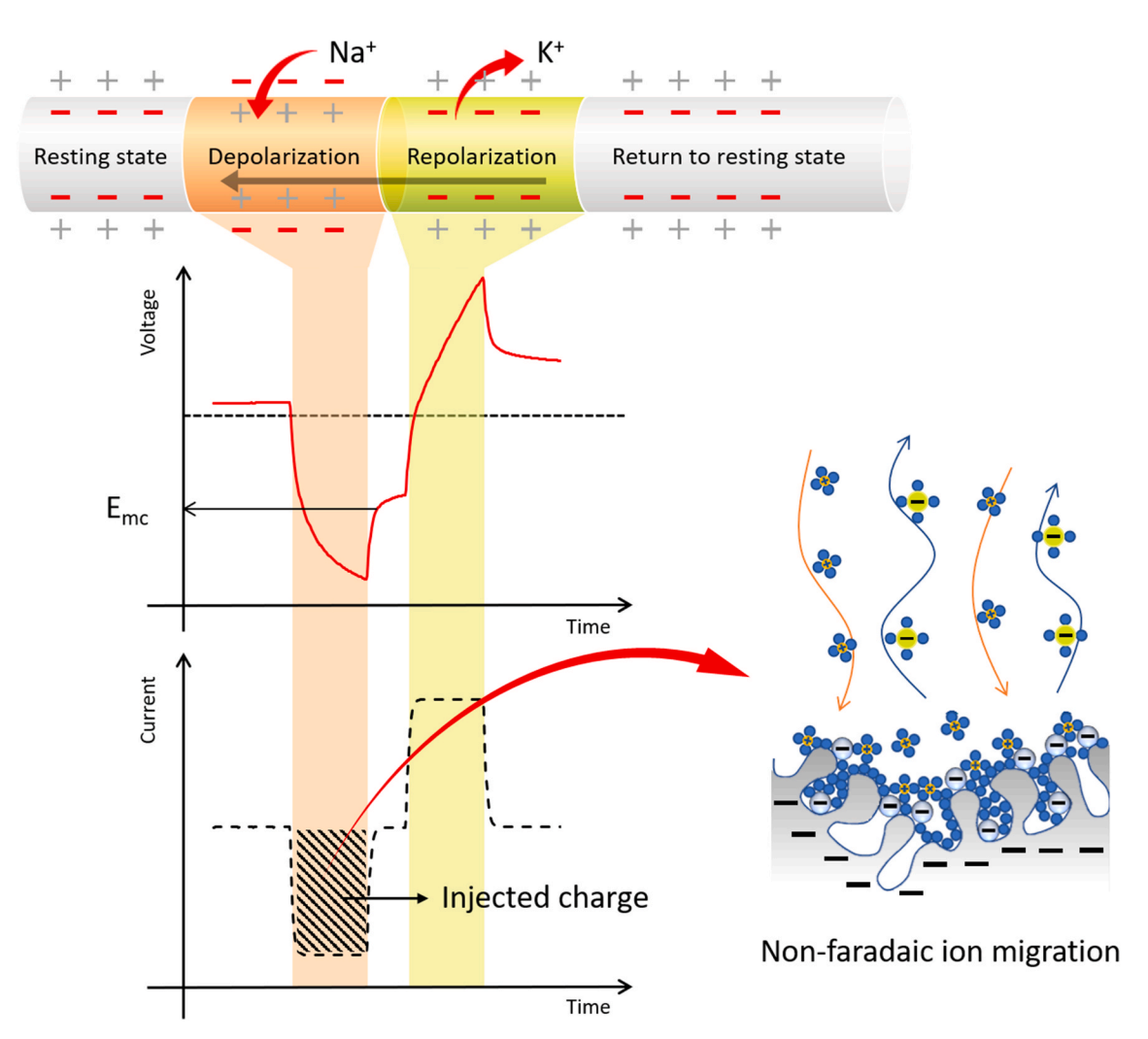
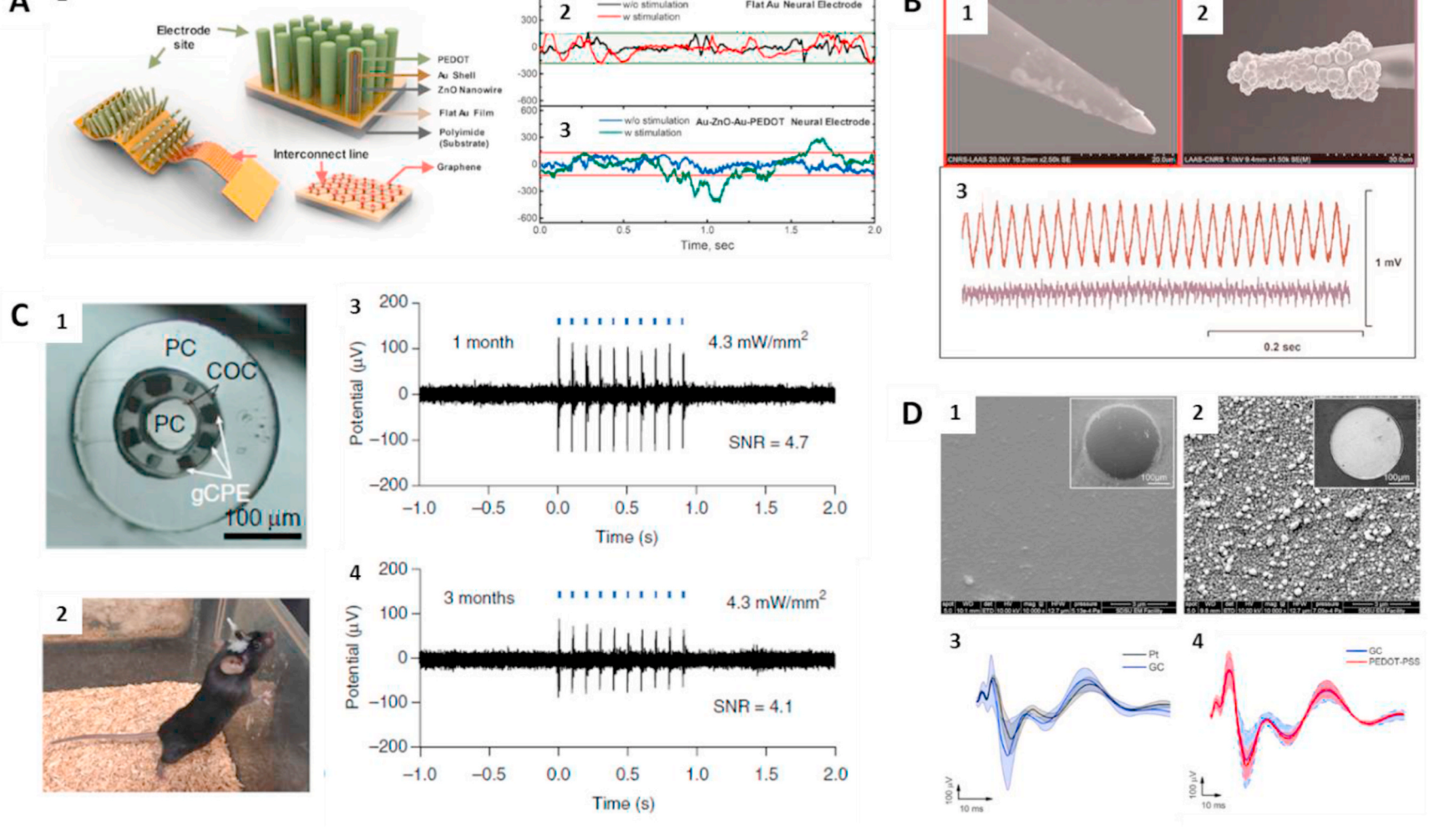


Fig. 2. Concept of biphasic stimulation with the symmetric cathodal first pulse and conceptual image of the electrode surface with a cathodal pulse.



- w/o stimulation

В

Flat Au Neural Electrode

1 A

Fig. 3. (A) Schematic diagram of the electrode based on the graphene and nanowire concept. (A-1) In vivo neural signal recorded by (A-2) Au electrode and (A-3) Au–ZnO–Au–PEDOT electrode for 2 s with and without whisker stimulation in the rat's brain (Ryu et al., 2017). (B) SEM images of identical commercial microelectrodes (B-1) and nano-structured (B-2). Electric hum recorded in a mouse brain slice maintained in vitro (B-3), by using commercial microelectrodes and nano-structured microelectrodes (Castagnola et al., 2015). (C) Cross-sectional microscopic image of the multi-modal fiber produced by thermal drawing. (C-1) A wild-type mouse implanted with a multi-functional probe. (C-2) Electrophysiological recording of optically evoked potentials in the mPFC of wild-type mice transfected with AAV5-CaMKIIα:ChR2-eYFP performed 1 month (C-3) and 3 months (C-4) after the one-step implantation and transfection surgery (Park et al., 2017). (D) SEM images of glassy carbon (D-1) and Pt electrode (D-2). Averaged somatosensory evoked potentials evoked by 100 stimuli for each 300 µm Ø Pt (black) and 300 µ m Ø GC (blue) microelectrodes (D-3) and each GC (blue) and GC-PEDOT-PSS (red) microelectrode (D-4) (Vomero et al., 2017). (For interpretation of the references to colour in this figure legend, the reader is referred to the Web version of this article.)

Table 1Electrochemical properties CP modified electrodes for neural recording and stimulation.

Surface modification	Substrate electrode	Impedance at 1 kHz (Mohm/μm²)	Charge storage capacity (CSC) (mC/cm ²)	Cyclic voltammetry (CV) scan condition	Charge injection limit (CIL) (mC/cm ²)	Ref
PPy/ClO ₄	Ir	35	160	(-0.9–0.5 V, 100 mV/s)	-	Abidian et al. (2010)
PEDOT/ClO ₄	Ir	13.5	240	(-0.9-0.5 V, 100 mV/s)	2.39	Abidian et al. (2010)
PEDOT/ionic liquid	Au	6	8.7	(-0.9-0.6 V, 1 V/s)	1.2	Du et al. (2015)
PEDOT:PSS	Pt	22	88.4	(-0.6-0.6 V, 50 mV/s)	3.6	Zhou et al. (2013)
PEDOT:PSS	Pt	-	7	(-0.9-0.5 V, 100 mV/s)	2.3	Cui and Martin (2003)
PEDOT:PSS	Au	9.2	-	_	-	Sessolo et al. (2013)
PEDOT/TFB ^a	Ir	7	-	_	-	Charkhkar et al. (2016)
PEDOT/pTS	Pt	_	_	_	2.1	Green et al. (2012)
PEDOT/MWCNT	Pt	17	202.9	(-0.6-0.6 V, 50 mV/s)	8.4	Zhou et al. (2013)
PPY/SLPF ^b	Au	222	_	_	_	Owen (2004)
PEDOT/DCDPGYIGSR	Pt	45	_	_	_	Green et al. (2009)
PPY/PSS/NGF ^c	Au	9	_	_	_	Kim et al. (2007)
PPY/glutamic acid	Indium tin oxide (ITO)	9.7	_	_	_	Kim et al. (2007)
PEDOT:PSS	Nerve, Pt/Ir	558.92	25.3 (cathodal)	(-0.6–0.8 V, 5 V/s)	-	Murbach et al. (2018)
PEDOT:PSS-rGO	Au	59	84.8	(-0.6-0.8 V, 50 mV/s)	6.91	Lee et al. (2019)
PEDOT:PSS coated MWCNT hydrogel	Alginate IPN, nickel- cadmium	200 kohm	1.2 (cathodal)	(-0.6-0.6 V, 500 mV/s)	-	Wang and Facchetti (2019)
PEDOT/pTS hydrogel	PVA-taurine, Pt/Ir	1180	212	(-0.8–0.6 V, 150 mV/s)	0.0158	Staples et al. (2018)
PEDOT/pTS hydrogel	PVA-taurine, Stainless steel	8560	85	(-0.8–0.6 V, 150 mV/s)	0.0135	Staples et al. (2018)
PEDOT/MWCNT	Pt/Ir	3.8	38	(-0.9-0.6 V, 1 V/s)	_	Alba et al. (2015)
PEDOT:PSS	GC	10.1736	893.5	(-0.8–0.6 V, 100 mV/s)	-	Vomero et al. (2017)
PEDOT:PSS	Au	67.52	2.55	(-0.6–0.8 V, 50 mV/s)	-	Qiang et al. (2017)
PEDOT:PSS	PEG hydrogel including CsA coated PLGA, Ti/Pt	$580.2 \pm 40.1 \; ohm$	0.267	(-0.65-0.8 V, 100 mV/s)	-	Heo et al. (2016)
PEDOT hydrogel	Poly (DMAA-co-5%MABP- co-2,5%SSNa), Ti/Pt/IrOx	_	26.5	(-0.6-0.8 V, 100 mV/s)	-	Kleber et al. (2017)
PEDOT/pTS hydrogel	PVA-taurine, Pt	1809.5	132	(-0.8–0.6 V, 150 mV/s)	-	Goding et al. (2017)
PEODT/pTS hydrogel	PVA-heparin, Pt	1732.5	80	(-0.8–0.6 V, 150 mV/s)	-	Goding et al. (2017)

a = tetrafluoroborate.

and biocompatibility are pursued as critically challenging issues. The long-term stability of coated CPs can be achieved by better integration with a substrate electrode. For example, PEDOT:PSS can be deposited on glassy carbon (GC) electrodes to perform long-term neural stimulation and low-noise recording (Vomero et al., 2017). When PEDOT:PSS was coated on GC electrodes, it was able to withstand 5 million biphasic pulses. They also showed twice of CSC compared to the PEDOT:PSS coated Pt electrodes. The reason is that GC electrodes form more coherent interaction with PEDOT:PSS than Pt electrodes.

An approach to ameliorate the biocompatibility of CPs is by utilizing surface modifications with biomolecules or biopolymer composites. CPs can also be made by naturally derived biomaterials such as melanin or polydopamine (PDA) (Kim and Nam, 2019; Kim et al., 2018, 2017; Xie et al., 2018). Kim et al. reported that PDA/PPy coatings on electrodes could reduce the impedance to be around half of that of PPy electrodes. The effect of electrical stimulation on PC12 neural cell growth confirmed the efficacy of the electrically CPs. A fraction of neurite-bearing cells on PPY increased from 23 to 32% whereas neurite formation on PDA/PPy notably increased from 24 to 57%. They demonstrated the potential *in vivo* applications of PDA/PPy-modified electrodes by implanting concentric needle electrodes in the tibialis anterior of a rat and measuring electromyography (EMG) signals. Signal to noise ratios (SNRs) of the EMG signals from the PDA/PPY electrodes

were found to be 1.3 and 2.9 times higher than those belonging to the PPY and bare electrodes, respectively. They also showed that PDA/PPy electrodes possess tissue compatibility by histological assessment of the subcutaneous tissues implanted with electrodes for four weeks.

Applying biopolymers as a substrate material for the CP coatings is another method for creating functional coatings. Marroquin et al. modulated the structure and the mechanical properties of the electrode by fabricating microfibrous electrodes using electrospun poly-L-lactic acid (PLLA), and these electrodes were coated with PEDOT to record electrical activity from rat's brain (Marroquin et al., 2018). The signals were recorded from acute hippocampal brain slices of adult rats for ex vivo studies and from the guinea pig auditory cortex using microfiber membrane electrodes for in vivo studies. For in vivo study, 3D-PEDOT strips which are composed of PEDOT-coated PLLA were used to record surface local field potentials (LFPs) from guinea pig auditory cortex, and responses including mean SNR were found to be analogous to those recorded using platinum ball electrode, while responses from nonconductive uncoated 3D-PLLA electrode were significantly lower. On the other hand, the extended contact of 3D-PEDOT mats on the rat's brain did not cause scarring for three weeks, whereas the Pt electrodes caused scarring due to their higher modulus than the surrounding tissue.

CPs are also fabricated in the form of hydrogels to mitigate the immune response triggered by differences in mechanical stiffness. Even

 $^{^{\}mathrm{b}}=\mathrm{silk}\text{-like}$ polymer having fibronectin fragments.

c = nerve growth factor.

though CP hydrogels do not show remarkable superiority over dense CPs in terms of their electrochemical performance, their low modulus makes CP hydrogels attractive for soft neural electrode materials. Staples et al. examined the effect of CP hydrogel coatings on electrochemical performances of the PtIr and stainless steel electrodes (Staples et al., 2018). 20 wt% Poly vinyl alcohol (PVA)-taurine hydrogel coating was performed on the PEDOT/p-toluene sulfonate (pTS) pre-coated electrodes. PEDOT was electrochemically polymerized through the PVA-taurine coating after photopolymerization. After coating with CP hydrogel, the impedance of PtIr and stainless steel at 1 kHz decreased to 1180 and 8560 $M\Omega \cdot \mu m^2$, respectively. Further, the CSC and CIL of CP hydrogel coated PtIr electrode were found to be 212 mC/cm^2 , 85 mC/cm^2 and that of stainless steel were 0.016 mC/cm², 0.014 mC/cm², respectively. At a current of 2 mA and frequency of 40 kHz, the CSCs of CP hydrogel coated stainless steel electrodes were reduced by 30% from their initial value at day 42, and there were no notable changes in impedance. Since the corrosion and delamination occurred on both coated and uncoated PtIr electrodes, they were found to be inappropriate for long-term stimulation.

Murbach et al. quantitatively analyzed the polymerization of PEDOT: PSS in agarose gel, followed by electrochemical in situ polymerization of PEDOT:PSS in peripheral nerves to fabricate a soft, precisely located injectable CP electrode for bi-directional communication (Murbach et al., 2018). The injectable intraneural PEDOT:PSS polymerization was performed in excised rat nerves using PtIr microwires with a diameter of 100 μm . The EDOT:PSS was injected at a constant rate of 0.2 $\mu L/min$ with a constant voltage of 2 V. Similar to in vitro test, in the nerve, the polymerization of PEDOT:PSS improved the electrochemical properties of the electrode. The presence of PEDOT:PSS not only lowered the impedance at 1 kHz by 10%, but also increased the CSC by 4.8 times compared to PtIR. In this study, they showed that PEDOT could be locally polymerized in individual peripheral nerves. For neural recording and stimulation applications, CPs are actively replacing metallic materials due to their far better electrochemical performances and biocompatibility.

3.2. Conducting polymers in regenerative engineering

CPs have been also used in the field of regenerative medicine in which tissue function is recovered or entirely replaced using scaffolds, bioactive molecules, and living cells (Talikowska et al., 2019). Porous scaffolds with CPs are fabricated as supporting templates for the growth and differentiation of cells which eventually leads to the formation of new tissue (Fig. 4). CPs can regulate cellular activities including cell growth (Collazos-Castro et al., 2010; Quigley et al., 2009; Wong et al.,

1994) and migration (Gumus et al., 2010) through electrical stimulation (Guo et al., 2013). Since controlling cellular behavior is pivotal for regeneration, CPs are attractive candidates as scaffold materials for regenerative engineering approaches. Polyacetylene (PA), PT, PEDOT, PPy, polyphenylene, and PANI are all examples of CPs that have shown promise of regenerative engineering (Guo et al., 2013). This section introduces regenerative applications of CPs for neural and cardiac tissues as well as bone regeneration and wound healing (Table 2).

3.2.1. Conducting polymers for neural regeneration

Significant effort has been made to regenerate injuries associated with the peripheral nervous system (PNS) and the central nervous system (CNS). Electrical, chemical, topological, and biological methods for incorporating stimuli into the polymer-based scaffolds have become critical for optimizing neural regeneration (Arino et al., 2008; Cao et al., 2009; Hamid and Hayek, 2008; Lee et al., 2009; Lu et al., 2008; Prabhakaran et al., 2009). Over the last decades, electrical stimuli have gained interest in promoting axon and neurite extension in vitro (Björninen et al., 2017) and nerve regeneration in vivo (Vivó et al., 2008). Since there are some limitations of CP-based biomaterials because of their low toughness, non-degradability, and difficulties in processing them into complex 3D structures (Park et al., 2009; Rivers et al., 2002; Wang et al., 2004; Zhang et al., 2007). hybrid materials have been developed. These hybrid materials typically employ a host polymer that provides the desired physical characteristics required, while the CP provides the electrically conductive characteristics to the resulting product. For instance, the bulk polymer may consist of biopolymers such as PLLA, chitosan (CS), gelatin, and cellulose (S. Wang et al., 2017e; Xu et al., 2016; Zhou et al., 2016).

Among the CPs used in neural regeneration applications, PPy was initially investigated because of its good biocompatibility and ability to support cell adhesion, electrical conductivity, easy preparation, and surface modification (Green and Abidian, 2015). Y. Zou et al. fabricated an aligned conductive PPy-PLLA fiber film with a diameter of about 800 nm and examined the effect of electrical stimulation of PC12 cells on this film (Zou et al., 2016). The surface resistivity of aligned PPy-PLLA fibers film was found to be 0.971 and 0.874 Ω m at the horizontal and lateral directions of the fiber axis, respectively, and no significant difference was observed in resistivity values. However, the surface resistivity of random PPy-PLLA fibers film was found to be 0.427 Ω m due to the lower porosity and higher amount of PPv nanoparticles on aligned PLLA fibers. Results showed that aligned PPv-PLLA fiber films could lead the extension of 68% PC12 neurites and also that extended distribution of neurites could be modified through aligned fibers film under electrical stimulation of 0-400 mV/cm. Since the results showed an improved

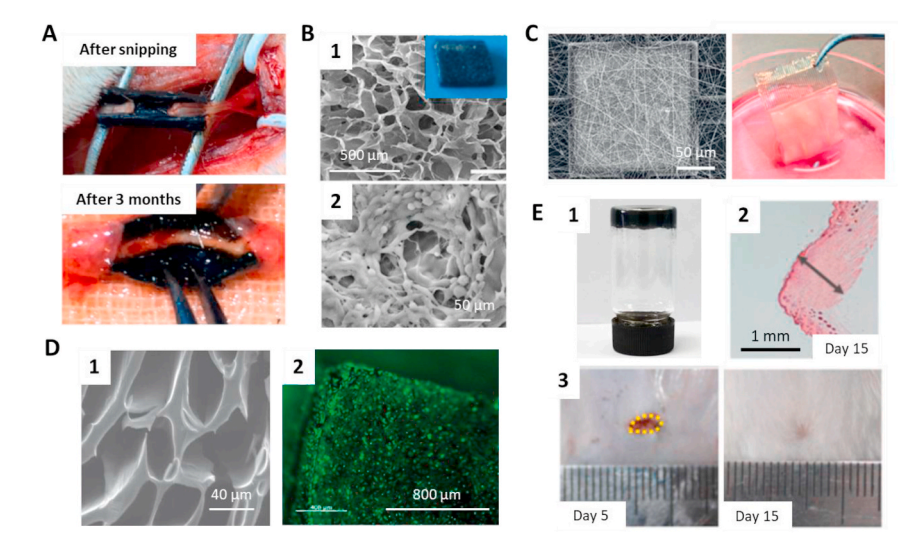


Fig. 4. (A) Photographs of the PANI/cellulose hydrogel composite conduit with snipped nerve and regenerated nerve for 3 months (Xu et al., 2016). (B) SEM image and photograph (inset) of polymerized PEDOT/CS/gelatin scaffolds (B-1), and SEM micrographs of cell-scaffold constructs after 3 days of culture (B-2) (S. Wang et al., 2017e). (C) SEM image of deposited electroactive polymer with polycaprolactone-gelatin fibers on the (left), and photograph of microelectronic cardiac patch after 7 days of cultivation with cardiac cells (right) (Feiner et al., 2016). (D) SEM image of poly (thiopheneacetic acid) hydrogel and fluorescent image of myoblast cells with visualization of active cell (D-2) on it following 3 days incubation (Mawad et al., 2012). (E) Photograph of amoxicillin loaded N-carboxyethyl CS/oxidized HA-graft-aniline tetramer hydrogel (E-1), granulation tissue thickness for on the 15th day (E-2), and photographs of wounds on 5th and 15th day for amoxicillin loaded HA-graft-aniline tetramer/N-carboxyethyl CS hydrogel dressing (E-3) (Qu et al., 2019).

Table 2Conducting polymers in regenerative engineering applications.

Material	Conductive Counterpart	Application	Conductivity	Mechanical Property	Cytocompatibility	Reference
OHA-AT/CEC hydrogel	Aniline tetramer	Wound Healing	~0.2 x10 ⁻³ S/ cm	1.4 kPa storage modulus	~1.1 times higher C2C12 myoblast proliferation than OHA/CEC	Qu et al. (2019)
GP/CMCS/OD hydrogel	PANI	Bone Regeneration	$6.7 \text{ x} 10^{-3} \text{ S/cm}$	5.71 MPa storage modulus	\sim 1.125 times higher C2C12 myoblast proliferation than G/CMCS/OD	(Longchao Li et al., 2015a)
BaG/Gel/PEDOT:PSS scaffolds	PEDOT	Bone Regeneration	1.7 x10 ⁻⁶ S/cm	_	~4 times higher hMSC ^a proliferation	Yazdimamaghani et al. (2015)
PANI/cellulose composite hydrogels	PANI	Neural Regeneration	$\begin{array}{l} 4.9\times10^{-1}\text{ S/}\\ cm \end{array}$	2.25 ± 0.05 MPa tensile strength $35.4\pm0.2\%$ elongation at break	\sim 2 times higher RSC96 cell proliferation	Xu et al. (2016)
rGO–PEDOT hybrid microfiber	rGO-PEDOT	Neural Regeneration	~2.52 S/cm	84 MPa tensile strength	~1.16 times higher MSC proliferation	Guo et al. (2016)
PEDOT/CS/Gel scaffold	PEDOT	Neural Regeneration	3.44 x10 ⁻² S/ cm	$49.8 \pm 3.1 \text{ kPa}$ compressive modulus	~1.3 times higher PC12 cell proliferation	(S. Wang et al., 2017e)
PEDOT-HA/CS/Gel scaffold	PEDOT	Neural Regeneration	3.16 x10 ⁻³ S/ cm	$47.3 \pm 0.3 \text{ kPa} \\ \text{compressive modulus}$	Support PC12 cell adhesion, Up-regulation of GAP43 and SYP protein and gene expression	(S. Wang et al., 2017d)
PPy-PLLA fiber film	PPy	Neural Regeneration	0.01 S/cm	100 MPa elastic modulus	Improved outgrowth and extended distribution of PC12 neurites	Zou et al. (2016)
PPy-PCL IPN network	PPy	Cardiac Regeneration	$\begin{array}{l} 0.001 \pm 0.0025 \\ \text{S/cm} \end{array}$	0.93 ± 0.19 GPa elastic modulus 0.071 ± 0.02 GPa hardness	Enhanced functional properties and maturation of HCL1 cardiomyocyte cells.	Spearman et al. (2015)
PPy/PCL/Gel nanofibrous scaffolds	PPy	Cardiac Regeneration	0.013 mS/cm	$16.8 \pm 1.9 \text{ MPa}$ tensile modulus	Higher cell adhesion and proliferation of cardiomyocytes	Kai et al. (2011)

^a = mesenchymal stem cell.

outgrowth and extended distribution of neurites, specifically under the electrical stimulation of 200 mV/cm, this aligned PPy-PLLA fiber film was proposed as a scaffold material for neural regeneration.

Graphene and its derivatives, graphene oxide (GO) and carboxy functionalized GO (CFGO), have been utilized in nerve regeneration studies to prepare composite materials with improved conductivity. Shang et al. employed GO and CFGO along with the sodium dodecyl benzenesulfonate (DBS) as dopants of PPy to produce conductive composite films for nerve repair studies (Shang et al., 2019). PPy with different dopants were electrochemically deposited on the surface of aligned PLLA fibers. In the presence of approximately 3.8% of GO, conductivity of DBS-GO-doped PPy-PLLA composite film with the fiber diameter of 2.51 µm reached to 32 S/cm. Due to the accumulated charges on the surface of GO sheets, DBS-GO-doped composite film showed the highest neurite length (149 µm) and alignment (70%) of PC12 cells under the electrical stimulation, when compared with DBS-CFGO-doped (137 µm, 64%) and DBS-doped (131 µm, 58%) composite films. They suggested that the composite films of PPy-PLLA prepared with the DBS and GO, can be used as a stable and cytocompatible matrix for nerve repair.

PANI is an attractive candidate because it is relatively cheap and possess better processability and stability as compared to PPy (Ning et al., 2018; Xia et al., 2013). Xu et al. fabricated PANI/cellulose composite hydrogels which exhibited 2.25 ± 0.05 MPa tensile strength, and 4.9×10^{-1} S/cm electrical conductivity (Xu et al., 2016). Results showed that the electrically conductive PANI could induce the proliferation of the Schwann cells on PANI/cellulose composite hydrogels nearly two times higher than that of the control group. They also indicated that most of the Schwann cells cultured on PANI/cellulose hydrogels showed their normal morphologies and attached to the hydrogel through the PANI sub-micrometer dendritic particles by cell pseudopods. Thus, the PANI/cellulose composite hydrogels were found to be biocompatible and could be used as nerve guidance conduits for the nerve-tissue repair.

Banisadi et al. prepared a conductive porous CS/gelatin matrix mixed with PANI/graphene nanoparticles for nerve regeneration. The initial conductivity of CS/gelatin matrix (10^{-7} S/cm) was enhanced to

0.182 S/cm with the addition of 10 wt% PANI/graphene nanoparticles, confirming the uniform distribution of highly conductive nanoparticles in porous matrix. They reported that the water retention capacity and porosity was decreasing while the electrical and mechanical properties were increasing with the addition of varied concentrations of PANI/graphene nanoparticles from 2.5 wt% to 10%. Cell proliferation studies performed with the Schwann cells, showed that the porous matrix with 2.5 wt% PANI/graphene has the highest number of attached cells. When taken together with this result, they chose scaffold with 2.5 wt% PANI/graphene as a suitable material for nerve tissue engineering.

PEDOT is another promising CP in neural regeneration applications. S. Wang et al. first synthesized hyaluronic acid (HA) doped PEDOT (PEDOT-HA) with a diameter of about 200 nm where HA improves the biocompatibility of PEDOT (S. Wang et al., 2017b). Then, the porous electroactive scaffold was fabricated by combining different amounts of conductive PEDOT-HA nanoparticles into a CS/Gelatin (Cs/Gel) matrix for nerve regeneration applications. They found that the incorporation of 8 wt% PEDOT-HA into scaffold provided 3.16×10^{-3} S/cm electrical conductivity, and 47.3 ± 0.3 kPa compressive modulus. When PC12 cell behavior in PEDOT-HA/Cs/Gel scaffolds was examined, the conductive scaffolds could support cell adhesion, viability, and higher expression of synapse growth genes. Based on their findings, they proposed PEDOT-HA/Cs/Gel scaffolds as candidates to be used in nerve tissue regeneration.

W. Guo et al. developed a step-driven self-powered neural differentiation system by combining PEDOT–reduced graphene oxide (rGO) hybrid microfibers and a triboelectric nanogenerator (TENG) (Guo et al., 2016). The electrical conductivity of the rGO microfiber (~1.51 S/cm) was significantly improved by compositing with 15% PEDOT (~2.52 S/cm). The tensile strength of the rGO microfiber was about 84 MPa for the 15% rGO–PEDOT hybrid microfiber at room temperature, indicating that the microfibers possess excellent mechanical properties and that the addition of PEDOT did not have any significant effect on the mechanical property of the microfibers. Live/dead cell assays revealed that after five days, the cell quantities on the 15% rGO–PEDOT hybrid microfibers were about ~1.16-fold higher than that on the rGO microfibers which was associated with better protein absorption ability of 15%

rGO–PEDOT hybrid microfiber than that of the rGO microfiber. The TENG gave a walking-induced voltage of 250 V, current of 30 μA and the transferred charge during one circuit of around 20 nC. When TENG electrical stimulation was applied, the expression of Tuj1 (a particular marker for neural cell) and GFAP (a particular marker for glial cell) on the 15% rGO–PEDOT hybrid microfiber was enhanced by $\sim\!1.68$ and $\sim\!1.5$ -fold over that on the rGO microfiber. These results indicated that the better electrical conductivity of the 15% rGO–PEDOT hybrid microfiber made the current transmission stronger, and the stronger charge injection increased neural proteins and gene expressions. In this study, rGO–PEDOT hybrid microfibers were shown to serve as effective scaffolds for MSCs proliferation and as a medium for step-driven TENG pulse electrical stimulation signals for inducing MSCs to differentiate into neural cells.

L. Weaver et al. also used PEDOT and GO to fabricate conducting polymer-based cell scaffolds by electrochemical coating. The biomolecules interferon-γ and platelet-derived growth factor that selectively promotes neuronal or oligodendrocyte lineage differentiation, respectively, were covalently cross-linked to the surface of the scaffolds through carboxylic acid functional groups on the surface of GO. The cell density of PEDOT/GO surface after seven days increased by 260% compared to after 30 minutes while the increase of cell density on the PEDOT/PSS surface during the period was only 30%. Moreover, neural stem cells grown on the interferon-γ and platelet-derived growth factor modified PEDOT/GO film through chemical crosslinking showed significantly more neuronal and oligodendrocyte differentiation respectively than cells grown on both an unmodified film and film modified with interferon-γ via nonspecific physical adsorption.

3.2.2. Conducting polymers for cardiac regeneration

Damaged cardiac tissue can be regenerated by applying cellular transplantation and 3D biomaterial scaffolds (Vunjak-Novakovic et al., 2010). One of the major drawbacks of tissue-engineered myocardial patches for the cardiac regeneration is that the extracellular matrix (ECM) cannot be mimicked functionally, because insulating polymeric scaffold hinders the signaling between cardiomyocytes (Kai et al., 2011). Optimized 3D scaffolds could be designed by conductive, biocompatible, and viscoelastic materials which are also functionalized with bioactive molecules or stem cells (Zia et al., 2016). CPs were considered as the potential candidates for enhancing the function of engineered cardiac tissue (Nezakati et al., 2018).

B. Spearman et al. prepared conductive PPy-polycaprolactone (PCL) interpenetrating networks (IPNs) and examined this matrix as a platform for guiding the production of functional cardiac cell sheets (Spearman et al., 2015). PPy-PCL was found to be suitable for culture of cardiomyocytes as an electrically-conductive substrate with a resistivity of $1.0\pm0.4~\rm k\Omega$ -cm, was similar to the resistivity of cardiac tissue (approximately 0.5 k Ω -cm). Cell culture tests performed with HCL1 atrial myocytes indicated that PPy-PCL IPNs improved the functional characteristics and maturation of cardiomyocyte cell sheets. Thus, they proposed to use conductive materials as active substrates for cardiac regeneration to functionally mimic the native cardiac tissue.

A. Gelmi et al., produced PPy coated poly (lactic-co -glycolic acid) PLGA fiber scaffolds which could transfer direct electrical and mechanical stimulation to induced human pluripotent stem cells (iPS) (Gelmi et al., 2016). These scaffolds showed no cytotoxic effects on the iPS and could serve as a microenvironments including both electrical and mechanical stimulation to improve proliferation and differentiation of the stem cells by tuning the biophysical and biochemical conditions of the transplanted cells and mimicking the natural structure of the heart.

Kai et al. fabricated PPy/poly (e-caprolactone)/gelatin (PPG) nanofibrous scaffolds by electrospinning with different concentrations of PPy to poly (e-caprolactone)/gelatin solution (Kai et al., 2011). They reported that increasing the concentration of PPy (0–30%) in the composite caused reduced fiber diameters from 239 ± 37 nm to 191 ± 45 nm and increased tensile modulus from 7.9 ± 1.6 MPa to 50.3 ± 3.3 MPa.

The conductivity of the PPG composite with 15% and 30% concentration of PPy scaffolds were obtained as 0.013 mS/cm and 0.37 mS/cm, respectively. Cardiomyocytes seeded on PPG nanocomposite with 15% PPy demonstrated significantly higher cell adhesion, proliferation, and increased expression of cardiac-specific proteins when compared with the poly (e-caprolactone)/gelatin scaffolds which did not contain any PPy.

3.2.3. Conducting polymers for bone regeneration

The native electrical properties of bone, discovered in 1950 (Fukada, 1956), allow external electric and electromagnetic stimulation to affect bone healing (Andrew et al., 1974; Darendeliler et al., 1997; Ryaby, 1998). Several studies have demonstrated the influence of stimulation on cell activities such as adhesion, proliferation (Meng et al., 2013), gene expression (Ozawa et al., 1989), and protein synthesis (Wang et al., 2006). Inspired by the idea of improving the bone healing with stimuli, the electrical property of the scaffolds could be adjusted by employing biocompatible CPs (Shahini et al., 2014).

L.Li et al. synthesized IPN conducting hydrogels with enhanced mechanical properties (Lanlan Li et al., 2015b). They used carboxymethyl-CS (CMCS) and gelatin-graft-PANI (GP) crosslinked with oxidized dextran (OD) to prepare IPN hydrogels. GP1 and GP2 with different PANI contents of 0.9 wt% and 1.8 wt% were synthesized to understand the effect of aniline content on the mechanical properties and cytotoxicity of the IPN hydrogels. The storage modulus of the gelatin/OD hydrogel was found to be about 1 kPa, and it increased to 924 kPa for the gelatin/CMCS/OD hydrogels. The GP1/CMCS/OD and the GP2/CMCS/OD hydrogels showed decreased moduli of about 571 kPa and 21 kPa, respectively. In principle, the increased crosslinking density causes the increment of the storage modulus. They related the decreased modulus of the GP/CMCS/OD hydrogel with the grafting reaction of PANI to gelatin which consumed amine group on the gelatin chains that lead to the crosslinking density reduced. The conductivity of the hydrogels varies as PANI content changes from gelatin/CMCS/OD to GP2/CMCS/OD. The conductivity of gelatin/CMCS/OD hydrogels was 6.2 mS/cm, attributed to the ionic conductivity of amino groups and carboxyl groups on the chains of gelatin and CMCS. With the incorporation of PANI into the hydrogels, the conductivity of GP1/CMCS/OD and GP2/CMCS/OD increased to 6.7 and 7.3 mS/cm, respectively. Adipose-derived mesenchymal stem cells (ADMSCs) and C2C12 myoblasts were used to test the cytotoxicity of the hydrogels and the results showed that the injectable CP hydrogels showed good cytocompatibility with ADMSCs and greatly enhanced the cell proliferation of C2C12 myoblasts. Based on these findings, the same group also synthesized biodegradable conductive copolymers based on polylactide and different amounts of (3, 6 and 10 wt%) aniline tetramer (PPGAT). These electroactive copolymers were found to be cytocompatible and the cell proliferation and osteogenic differentiation from bone marrow-derived mesenchymal stem cells (BMSCs) were significantly enhanced. Especially, PPGAT films which contain 6 wt% aniline tetramer showed the best proliferation performance, demonstrating that the suitable AT content was an important factor for cell proliferation.

Another study was performed by M. Yazdimamaghani et al. where hybrid conductive scaffolds prepared by adding different amounts of PEDOT:PSS in the composition of gelatin and bioactive glass scaffolds (Yazdimamaghani et al., 2015). Results showed that addition of 0.3% (w/w) PEDOT:PSS in the mixture of 10% (w/v) gelatin and 30% (w/v) bioactive glass can increase the conductivity from 100 to 170 $\mu S/m$ and the cell viability more than 4 times compared to a nonconductive composition.

3.2.4. Conducting polymers for wound healing applications

Skin plays a vital role in protecting the body from external damage and microbial invasion. Thermal burn wounds generate approximately 265,000 deaths each year (Jahromi et al., 2018). Various biomaterials for wound dressing with excellent antibacterial activity have been

studied (GhavamiNejad et al., 2016; Ma et al., 2017; Zhou et al., 2017). Particularly, conductive materials have a positive effect on improving the cellular activities of fibroblasts and keratinocytes (Guo and Ma, 2018). Qu et al. designed biodegradable injectable conductive anti-oxidant hydrogel dressing by mixing the biocompatible polymer N-carboxyethyl CS (CEC) and oxidized HA-graft-aniline tetramer (OHA-AT) polymer under physiological conditions (Qu et al., 2019). To provide antibacterial activity, they also loaded hydrogels with the antibiotic amoxicillin (D-OHA-AT10/CEC) and compared the in vivo wound healing performance with the commercial product, TegadermTM. OHA-AT polymers were prepared with different amounts of AT which were OHA, OHA-AT5, OHA-AT10, OHA-AT15, and OHA-AT20. The conductivity of OHA/CEC hydrogel was found to be 0.05 mS/cm which was increased to 0.09 mS/cm and 0.42 mS/cm with the addition of AT segments. Based on the C2C12 myoblast cell proliferation and LIVE/-DEAD staining results, they reported that OHA-AT5/CEC and OHA-AT10/CEC hydrogels had better cytocompatibility than OHA/CEC. Furthermore, the amoxicillin loaded group D-OHA-AT10/CEC hydrogel showed antibacterial performance and the best treatment effect than all the experimental groups. In this study, the role of the AT addition on the conductivity of the hydrogels was demonstrated and correlated with improved wound healing.

CPs were easily blended with biocompatible or biodegradable polymers such as PLLA, cellulose, CS, and gelatin. Thus, biocomposite CPs became preferable regenerative materials for neural regeneration, cardiac regeneration, bone regeneration, and wound healing applications. Furthermore, functional molecules such as growth factors and specific genes have been loaded to CPs composites to improve the regenerative performances of the materials.

3.3. Artificial tissue - sensors and actuators

Though applied prostheses or artificial tissues are currently used as replacements for malfunctioned organs or tissue such as bone, joint, cochlear, and limbs, development of prosthesis with advanced humanbody interfaces aims to assist humans by enabling them to have superior abilities, such as lifting heavy weights or detecting a wider range of visions, sounds, and smells. However, there are significant drawbacks of conventional metallic materials (Castagnola et al., 2015). CPs can offer improved integration between biological tissues and electrical devices based on their outstanding electrochemical performances, biocompatibility, and processability. Therefore, most studies adopting CPs focus on providing a lightweight, stretchable and flexible mechanical properties, enhanced sensing abilities, and various controlled actuation to the artificial sensors and actuators in order to mimic the native tissue both physically and functionally. Biological tissues can behave as either sensors or actuators like skin and muscle; however, for more complex tissues, organs, for example, act as a combination of sensors and actuators. Therefore, currently developed prototypes of artificial tissues are being fabricated as a composition of sensors or actuators (Fig. 5).

3.3.1. Electronic skin (E-Skin)

Human skin plays a role as the broadest organ in our bodies, and it receives various stimuli from the surrounding environment. External physical stimulations received through receptors of various sensory nerves embedded within the skin, for example, pressure, vibration, and temperature, are converted into the physiological signals and transmitted to the brain (Hammock et al., 2013). Electronic skin (e-skin) may refer to the skin-mimetic integrated sensor array into a wearable film with flexibility and stretchability by dispersing the conductive fillers to an elastomeric matrix (Wang et al., 2019, 2020; Zhu et al., 2016). For conductive fillers, conventional metals, liquid metals, carbon nanomaterials have been commonly used (Wang and Facchetti, 2019). Liquid metal can function as a conducting path while encapsulated in a microfluidic channel (Kang et al., 2018). Conventional stretchable conductive materials were achieved by nano-scale distribution,

orientation, and connectivity of nanofillers. Among nanofillers carbon nanomaterials are popular. However, their percolation-dependent conductivity and the poor solubility in most solvent remains a hurdle (Chen et al., 2013; Chiou et al., 2018; Wang et al., 2013). CPs are advantageous because chemical modification can create versatile stimuli-responsive transduction for both physical and chemical changes, such as temperature (Hong et al., 2016; Trung et al., 2016; Vuorinen et al., 2016), pressure (Darabi et al., 2017; Wang et al., 2018), humidity (Park et al., 2018), pH (Kim et al., 2016; Rahimi et al., 2017, 2016), and diverse set of target molecules (Lanlan Li et al., 2015b; Li et al., 2018; Liu et al., 2018; Pal et al., 2018). Also, the processability of CPs can cast into macro-shapes such as films, fibers, and hydrogels via precision tools, including 3D printer (Fu et al., 2018).

CP is an inherently rigid material. Thus, molecular engineering is required for stretchable e-skin applications. Table 3 provides the list of CP based materials in e-skin applications. CPs can be blended with elastomeric polymers to obtain stretchability. Taroni et al. blended PEDOT:PSS with a commercial elastomeric polyurethane (PU) to improve the stretchability (Taroni et al., 2018). The strain of a blend containing 90 wt% of PU reached to ~700% while maintaining conductivity of 79 ± 5 S/cm. Rigid CPs can also be softened by injecting ionic additives. Wang et al. added ionic additives to PEDOT:PSS in order to partially soften polymer chains to create soft domains to achieve high fracture strain (Y. Wang et al., 2017b). The compounds reduced Young's moduli of PEDOT:PSS bulk film by 50 times while preserving its conductivity of 3600 S/cm after 1000 cycles to 100% strain. Teo et al. also used 1-ethyl-3-methylimidazolium tetracyanoborate (EMIM TCB), an ionic liquid, to fabricate the stretchable and semitransparent PEDOT: PSS film (Teo et al., 2017). The EMIM TCB acts as a plasticizer as well as a secondary dopant. As a result, the conductivity reached to >1000 S/cm with a stable performance at elongation up to 180% in combination with the prestrained substrate technique.

CP hydrogel can be stretchable. Gan et al. fabricated sandwich-like PDA-grafted and sulfonated graphene oxide (PSGO)-PEDOT nanosheets by templating with functionalized graphene (Gan et al., 2020). This PSGO-PEDOT was used as nanofillers to construct adhesive CP hydrogel, which adheres to diverse materials such as metal, ceramic, and bio-organ. However, the conductivity of the CP hydrogel was relatively poor, which was measured to be 1.08 S/cm. CP hydrogel can be fabricated without matrix. Lu et al. reported pure PEDOT:PSS hydrogels with an interconnected nanofibril network (B. Lu et al., 2019a) by a dry-annealing process. During the process, PEDOT:PSS is recrystallized by elevated temperature and dimethyl sulfoxide (DMSO).

Stretchable CPs are highlighted by multi-properties, such as physical and chemical sensing, biodegradability, and self-healing ability. Lu et al. demonstrated the self-healable property with poly (2-acrylamido-2-methyl-1-propanesulfonic acid), PANI, and phytic acid by a simple two-step method as an e-skin (Y. Lu et al., 2019b). This e-skin stretched omnidirectionally over 1900% and their repeatable recovery was over 98% of conductivity. Cycling stability was demonstrated by the repetition tests of 70 loading-unloading cycles at 20% strain. When the sensors were applied to the wrist, finger, knee, and elbow, the different motions were distinguished by the resistance change.

E-skins have the potential to give hyper-enhanced abilities to detect molecules or chemicals that cannot be felt by natural skin. Vitoria et al. reported a low-cost and scalable method to prepare patterned PPy nanofilms on the cellulose substrates by *in situ* gas-phase polymerizations (de Morais et al., 2019). The electrical resistance of the PPy nanofilms was able to be tuned by NaOH, which induces the deprotonation. Consequently, the sensor could map both liquid-state and gas-state HCl on the e-skin.

Stretchable CPs are focusing on the engineering of material properties with physicochemical tunability (Fan et al., 2014; Guan et al., 2018). Thus, CPs can simplify and miniaturize the integrated e-skin platform without further assembly steps. However, PEDOT:PSS materials have been predominantly chosen as e-skin among a wide selection

10

В

C

Fig. 5. (A) Principle of conjugated polymer bending actuators based on the oxidation-reduction process of PPy (Khaldi et al., 2016). (B) Pictures and schemes of the angular displacements described by the PPy-Br/PPy-dodecyl DBS artificial muscle by the voltammetric and coulo-voltammetric responses (Fuchiwaki et al., 2015). (C) Patterned PEDOT/STEC film on SEBS (top) and the film being stretched (bottom). The line width is 1 mm (Y. Wang et al., 2017b). (D) Merged images of two actuation positions (±2 V at 1 Hz) of a dragonfly with actuators produced by drop-casting and cutting (Simaite et al., 2015). (E) Photographs of the reversible opening and closing processes of an artificial flower based on the aligned multi-walled carbon nanotube (MWCNT)/poly [1-phenyl-2-(p-trimethylsilyl) phenylacetylene] composite driven by ethanol (Lu et al., 2014). (F) The device was transferred onto the rough surface of an avocado (Scale bar: 10 mm). (G) The device transferred onto a polydimethylsiloxane (PDMS) substrate for electrical measurement (Scale bar: 5 mm) (Lei et al., 2017).

Table 3CP based materials that can be utilized in future applications of e-skin.

Conducting polymer	Matrix	Туре	Maximum Conductivity (S/cm)/ Lowest Surface Resistance (ohm/ sq)	Maximum Stretchability	Ref
PANI	Nitrile-butadiene rubber	Sponge	$1.10\times10^{-4}~\text{S/cm}$	250%	Luan et al. (2017)
PEDOT:PSS	PDMS	Film	20 Ω/sq	95%	Li et al. (2019)
PEDOT:PSS	poly (methacrylic acid) grafted PDMS	Coating	90 Ω/sq	100% (~90 Ω/sq)	Oh et al. (2016)
PEDOT:PSS	PEDOT:PSS/TritonX-100	Dough	78 S/cm	57% (~16 Ω/sq)	Li et al. (2019)
PEDOT:PSS	PEDOT:PSS/EMIM TCB	Film	1280 S/cm	180% (~160 Ω/sq)	Teo et al. (2017)
PEDOT	PEDOT:PSS/Poly (ethylene glycol) methacrylate (PEDMA)	Composite	$3.1 \times 10^4 \Omega/\text{sq}$	400% (2.5 × 10^7 Ω/sq)	Kim et al. (2020)
PANI	acrylamide (AAm), graphen oxide (GO) and CS (CS)	Hydrogel	0.03 S/cm	360%	Jin et al. (2020)
PPy	Silicone rubber	Composite	Not mentioned in the manuscript	100%	Kurian et al. (2020)
PEDOT:PSS/PEG	Micro-cracked Au/PDMS	Coating	${\sim}1~\text{k}\Omega$ (at 1 kHz)	40% (~1.4 × 10 ⁴ kΩ at 1 kHz)	Decataldo et al. (2019)
PEDOT:PSS/4-(3-butyl-1- imidazolio)-1-butanesulfonic acid triflate (BIBSAT)	PEDOT:PSS/4-(3-butyl-1-imidazolio)-1- butanesulfonic acid triflate (BIBSAT)	Aerogel	77.4 × 4.0 S/cm	-80 to 100%	Chen et al. (2019)
PPy	PEG methyl ether methacrylate-based polymer	Composite	0.88 S/cm	410%	Chen et al. (2019)
PEDOT:PSS	polyurethane	Composite	$79 \pm 5 \text{ S/cm}$	700%	Taroni et al. (2018)
PEDOT:PSS	Wrinkled PDMS	Coating	1400 Ω/sq	100% (4630 Ω/sq)	Wen et al. (2018)
PANI	PU microfibrous membrane	Coating	0.1 S/cm	50%	Jeon et al. (2018)
PEDOT:PSS	PEDOT:PSS/ionic additives—assisted stretchability and electrical conductivity (STEC) enhancers	Film	4100 S/cm (at 100% strain)	600% (100 S/cm)	Y. Wang et al. (2017b)
PEDOT:PSS	PDA-grafted and PSGO	Hydrogel	1.08 S/cm	-80 to 2000%	Gan et al. (2020)
PEDOT:PSS	PEDOT:PSS/DMSO	Hydrogel	20 S/cm	35% (~20 S/cm)	B. Lu et al. (2019a)

of CPs, which restrict the potential to overcome the current limitations such as toxicity and chronic biocompatibility to replace bio-skin.

3.3.2. Electronic muscle (E-Muscle)

CPs also have the potential to act as soft mechanical actuators in biomedical applications. Properties such as lightweight, flexibility, biocompatibility, low driving voltages, high actuation strain and actuation power, and fast response speed are required for materials used as soft actuators. Currently reported functional materials including elastomers (Anderson et al., 2012), carbon nanotubes (CNTs) (Lima et al.,

2012), and shape-memory polymers (Leng et al., 2011) have not yet fully met these needs. Some examples of the use of CP-based materials as soft actuators and some metrics of their performance are shown in Table 4.

Two representative mechanisms of volume variation of electroactive materials are electro-chemo-mechanical coupling, which involves ion exchange, and electro-thermal-mechanical coupling, which uses water molecule exchange by Joule heating. The typical structure of a polymeric actuator is a bilayer structure, one side of which is made of CP while the other side is made of metal, plastic, or another CP, which has

Table 4Currently developed CP-based soft actuators and their actuating performances.

Materials	Driven force	Maximum actuation force	Maximum actuation strain (%)	Response time (s)	Operating condition	ref
PEDOT:PSS/MWCNTs	0-2.5 V	1.43 mN	0.64	0.072	in air	Wang et al., (2017a)
Ethylene glycol (EG)/ PEDOT:PSS/EG fiber	0–5 V	22 MPa	0.4	0.5	in air	Zhou et al. (2016)
PEDOT:PSS/PVDF	0-1.5 V	_	>0.6	10	in air	Simaite et al. (2015)
PEDOT:PSS/paper	Humidity (15%,85%)	5.58 mN	0.3	18	in air	Hamedi et al. (2016)
PEDOT:PSS film	0-10 V	17 MPa	2.4-4.5	20	in air	Okuzaki et al. (2009)
PPy $(BF_4)_{0.33}$ $(H_2)_{0.25}$ film	0–3 V	8.9 MPa	1	50	in air	Okuzaki et al. (2013); Okuzaki and Kunugi (1998)
PEDOT:PSS/PVA blended fiber	0–8 V	11 MPa	0.12	50	in air	Miura et al. (2014)
PEDOT semi-IPN hollow fiber	0–1 V	<1 MPa	3	80	in air	Plesse et al. (2010)
PEDOT/PEO ^a /NBR ^b IPN	0-2 V	0.18 N	0.5	600	in air	Fannir et al. (2019)
PEDOT/PEO/NBR IPN	0–2 V	-	0.2	600	under vacuum (1.4 \times 10 ⁻⁴ mBar)	Fannir et al. (2019)

^a = polyethyleneoxide.

^b = nitrile butadiene rubber.

volume expanding variations. Fuchiwaki et al. used PPy-Br film as an anion exchange layer and PPy-DBS as a cation exchange layer to fabricate an asymmetric bilayer muscle (Fuchiwaki et al., 2015). During oxidation, the PPy-Br layer swelled by the entrance of anions and water induced by the increase of Br-concentration in the film and PPy-DBS layer shrank. On the contrary, during reduction, the PPy-Br layer pulled on the bilayer and PPy-DBS layer pushed on the bilayer. The reversible angular displacement during the voltammetric cycle was 200° . Since it was close to a linear function of the consumed charges, the cooperative dynamic effect was quantified by the angle per unit of consumed charge: $2.35^{\circ}/mC$ for the PPy-Br/PPy-DBS bilayers.

Inkjet-printed PEDOT:PSS bending bilayer actuators were fabricated by Simaite et al. (2015). There are challenges to inkjet print of CPs due to their rheological properties (De Gans et al., 2004; Derby, 2010; Goldin et al., 1969) and complex solution-membrane interactions which lead to typically poor adhesion or uncontrolled infiltration (Angelo et al., 2012; Simaite et al., 2015). Challenges involved in inkjet printing of PEDOT: PSS were overcome through secondary doping with 5 vol% of ethylene glycol that improved the conductivity and mechanical properties of the film. The ethylene glycol doped PEDOT:PSS suspension was printed on the hydrophilic hybrid polyvinylidene fluoride (PVDF)/PVDF-graft-polyethylene glycol methacrylate (PEGMA) membranes without infiltration. After printing 10 layers of PEDOT:PSS on both sides of the membrane, the actuating performances were demonstrated. The peak-to-peak strain was more than 0.6% when the actuation with 1.5 V square wave at 50 mHz was applied.

Conductive soft actuators can be used as scaffold materials for cardiac regeneration to provide both tight integrations and effective signal transductions with a tissue. Wang et al. fabricated PLLA/PANI conductive nanofibrous sheets with an extracellular matrix-like nanostructure by electrospinning method (L. Wang et al., 2017). To mimic the structure of the myocardium extracellular matrix, the diameter of electrospun fibers was maintained at nearly 500 nm even after the PANI coating. The nanofibrous structure and electrical conducting properties of PLLA/PANI composites showed a synergetic effect on the promotion of myotube number and length, maturation, and fusion index. Moreover, the sheets laden with cardiomyocytes could form 3D bioactuators with tubular and folding shapes. In Dulbecco's Modified Eagle Medium, PLLA/PANI sheets spontaneously contracted at 1.6 Hz and showed 6.9 μm displacement with the synchronous beating of the cardiomyocytes. PLLA/PANI sheets also supported the synchronous beating with superior electrical cell-cell coupling than PLLA nanofibrous sheet. At the moment, CP possesses a leading position due to their processability and voltage-driven chemo-mechanical swelling characteristics. However, as the development of soft actuator using CP is still at the emerging level, study for operating complex motions and mechanical functions through multi-channel configuration is needed.

4. Conclusions

CPs have gained considerable attention and are being exploited in a variety bioelectronic applications, including biosensors, drug delivery systems, artificial muscles, and neural interfaces. In this review, we discussed the recent progress of CPs in bio-interfacing electronics, focusing on three specific applications: neural recording and stimulation, regenerative bioengineering, and e-skin and e-muscle. For neural recording and stimulations, although the introduction of synthetic CPs is rapidly replacing the metallic materials, lowering electrochemical impedances and improving long-term durability and biocompatibility remain demanding tasks. In regenerative engineering, both the biomolecule-decorated CP and the CP-coated bio-scaffold showed excellent performance for regenerating cardiac tissues or nerve tissues. However, regenerative engineering still requires biodegradability as well as complete biocompatibility with tissues, which is a difficult challenge to satisfy by synthetic CP. E-skin may refer to the stretchable and integrated multiple sensor arrays that can be newly applied to robotics. To date, no single material achieve the full potential of human skin function. However, CPs can be engineered to be stretchable, flexible, and tunable like human skin to act as a multiphasic sensor. Emuscle, on the other hand, refers to a soft mechanical actuator that requires lightweight, flexibility, biocompatibility, low driving voltages, fast response speed, and high actuation strain and actuation power. The processability of CPs and their voltage-driven chemo-mechanical swelling characteristics can be unique advantages over conventional conducting materials. CP shows fast reaction speed and efficient energy conversion ability. However, just simple dynamic performances on the actuators were implemented by CPs, which naturally requires further studies.

While CPs can be successfully engineered as stretchable, tunable, conformable soft bio-interfaces, PEDOT, PANI, and PPy have been dominantly used. Thus, the versatility of CPs is not fully exploited yet. Thus, novel CPs, including but not limited to bio-hybrid CPs, biocomposite CPs, and naturally derived materials, should be further tested for finding their proper uses in the field, particularly for solving current technical challenges, including physically seamless matching, safe bioactivity, chronic bio-functionality without compromising electrical conductivity at the biotic - abiotic interfaces. Natural conjugated biomaterials, including melanin and polydopamine, need to be further studied as a future candidate for biocompatible bioelectronic interface materials.

Declaration of competing interest

The authors declare that they have no known competing financial interests or personal relationships that could have appeared to influence the work reported in this paper.

Acknowledgment

This work was funded by the National Research Foundation of Korea (NRF-2018K1A3A1A32055149, NRF-2017R1A2B4012736, and NRF-2020R1F1A1075944). Support was also provided by the MSIT-Air Force Office of Scientific Research Program for Materials and Next Generation Nanosystems, and the National Science Foundation (DMR-1808048).

References

```
Abidian, M.R., Corey, J.M., Kipke, D.R., Martin, D.C., 2010. Small 6, 421–429. Akieh-Pirkanniemi, M., Lisak, G., Arroyo, J., Bobacka, J., Ivaska, A., 2016. J. Membr. Sci. 511, 76–83.
```

Alba, N.A., Du, Z.J., Catt, K.A., Kozai, T.D., Cui, X.T., 2015. Biosensors 5, 618–646. Anderson, I.A., Gisby, T.A., McKay, T.G., O'Brien, B.M., Calius, E.P., 2012. J. Appl. Phys. 112, 041101.

Andrew, C., Bassett, L., Pawluk, R.J., Pilla, A.A., 1974. Science 184, 575–577. Angelo, P.D., Farnood, R.R., Sodhi, R.N., Cole, G.B., 2012. Nord. Pulp Pap. Res. J. 27,

Arino, H., Brandt, J., Dahlin, L.B., 2008. Scand. J. Plast. ReConstr. Surg. Hand Surg. 42, 281–285.

Arroyo, J., Akieh-Pirkanniemi, M., Lisak, G., Latonen, R.-M., Bobacka, J., 2019. J. Membr. Sci. 581, 50–57.

Ateh, D., Navsaria, H., Vadgama, P., 2006. J. R. Soc. Interface 3, 741–752.

Ates, M., 2011. Prog. Org. Coating 71, 1–10.

Baraldi, P., Capelletti, R., Crippa, P., Romeo, N., 1979. J. Electrochem. Soc. 126, 1207. Baughman, R., Shacklette, L., 1991. Sci. Appl. Conduct. Polym. 47.

Bettinger, C.J., Bruggeman, J.P., Misra, A., Borenstein, J.T., Langer, R., 2009. Biomaterials 30, 3050–3057

Bidez, P.R., Li, S., MacDiarmid, A.G., Venancio, E.C., Wei, Y., Lelkes, P.I., 2006.
J. Biomater, Sci. Polym. Ed. 17, 199–212.

Björninen, M., Gilmore, K., Pelto, J., Seppänen-Kaijansinkko, R., Kellomäki, M., Miettinen, S., Wallace, G., Grijpma, D., Haimi, S., 2017. Ann. Biomed. Eng. 45, 1015–1026.

Bredas, J.L., Street, G.B., 1985. Acc. Chem. Res. 18, 309-315.

Cao, H., Liu, T., Chew, S.Y., 2009. Adv. Drug Deliv. Rev. 61, 1055-1064.

Castagnola, V., Descamps, E., Lecestre, A., Dahan, L., Remaud, J., Nowak, L.G., Bergaud, C., 2015. Biosens. Bioelectron. 67, 450–457.

Chang, J.-F., Sun, B., Breiby, D.W., Nielsen, M.M., Sölling, T.I., Giles, M., McCulloch, I., Sirringhaus, H., 2004. Chem. Mater. 16, 4772–4776.

Charkhkar, H., Knaack, G.L., McHail, D.G., Mandal, H.S., Peixoto, N., Rubinson, J.F., Dumas, T.C., Pancrazio, J.J., 2016. Acta Biomater. 32, 57–67.

- Chen, Y., Tao, J., Deng, L., Li, L., Li, J., Yang, Y., Khashab, N.M., 2013. ACS Appl. Mater. Interfaces 5, 7478–7484.
- Chen, G., Rastak, R., Wang, Y., Yan, H., Feig, V., Liu, Y., Jiang, Y., Chen, S., Lian, F., Molina-Lopez, F., 2019. Matter 1, 205–218 others.
- Chen, J., Liu, J., Thundat, T., Zeng, H., 2019. ACS Appl. Mater. Interfaces 11, 18720–18729.
- Chiou, K., Byun, S., Kim, J., Huang, J., 2018. Proc. Natl. Acad. Sci. Unit. States Am. 115, 5703–5708.
- Ciucci, F., 2019. Curr. Opin. Electrochem. 13, 132-139.
- Cogan, S.F., 2008. Annu. Rev. Biomed. Eng. 10, 275-309.
- Collazos-Castro, J.E., Polo, J.L., Hernández-Labrado, G.R., Padial-Cañete, V., García-Rama, C., 2010. Biomaterials 31, 9244–9255.
- Cui, X., Martin, D.C., 2003. Sensor. Actuator. B Chem. 89, 92-102.
- Darabi, M.A., Khosrozadeh, A., Mbeleck, R., Liu, Y., Chang, Q., Jiang, J., Cai, J., Wang, Q., Luo, G., Xing, M., 2017. Adv. Mater. 29, 1700533.
- Darendeliler, M.A., Darendeliler, A., Sinclair, P.M., 1997. Int. J. Adult Orthod. Orthognath. Surg. 12, 43–53.
- De Gans, B.-J., Duineveld, P.C., Schubert, U.S., 2004. Adv. Mater. 16, 203-213.
- de Morais, V.B., Corrêa, C.C., Lanzoni, E.M., Costa, C.A.R., Bufon, C.C.B., Santhiago, M., 2019. J. Mater. Chem. A 7, 5227–5233.
- Decataldo, F., Cramer, T., Martelli, D., Gualandi, I., Korim, W.S., Yao, S.T., Tessarolo, M., Murgia, M., Scavetta, E., Amici, R., others, 2019. Sci. Rep. 9, 1–9.
- Derby, B., 2010. Annu. Rev. Mater. Res. 40, 395-414.
- Ding, R., Lisak, G., 2019. Anal. Chim. Acta 1091, 103-111.
- Ding, R., Krikstolaityte, V., Lisak, G., 2019. Sensor. Actuator. B Chem. 290, 347–356.
- Du, Z.J., Luo, X., Weaver, C.L., Cui, X.T., 2015. J. Mater. Chem. C 3, 6515–6524.
- Eom, T., Woo, K., Cho, W., Heo, J.E., Jang, D., Shin, J.I., Martin, D.C., Wie, J.J., Shim, B. S., 2017. Biomacromolecules 18, 1908–1917.
- Eom, T., Jeon, J., Lee, S., Woo, K., Heo, J.E., Martin, D.C., Wie, J.J., Shim, B.S., 2019. Part. Part. Syst. Char. 36, 1900166.
- Fan, J.A., Yeo, W.-H., Su, Y., Hattori, Y., Lee, W., Jung, S.-Y., Zhang, Y., Liu, Z., Cheng, H., Falgout, L., others, 2014. Nat. Commun. 5, 1–8.
- Fannir, A., Temmer, R., Nguyen, G.T., Cadiergues, L., Laurent, E., Madden, J.D., Vidal, F., Plesse, C., 2019. Adv. Mater. Technol. 4, 1800519.
- Feiner, R., Engel, L., Fleischer, S., Malki, M., Gal, I., Shapira, A., Shacham-Diamand, Y., Dvir, T., 2016. Nat. Mater. 15, 679–685.
- Fu, X., Zeng, W., Ramírez-Pérez, Á.C., Lisak, G., 2018. Chem. Commun. 54, 980–983. Fuchiwaki, M., Martinez, J.G., Otero, T.F., 2015. Adv. Funct. Mater. 25, 1535–1541.
- Fukada, E., 1956. J. Phys. Soc. Jpn. 11, 1301A–1301A. Gan, D., Huang, Z., Wang, X., Jiang, L., Wang, C., Zhu, M., Ren, F., Fang, L., Wang, K.,
- Gain, D., Huang, E., Wang, K., Jiang, L., Wang, C., Zhu, M., Ich, F., Fang, E., Wang, K. Xie, C., 2020. others. Adv. Funct. Mater. 30, 1907678.

 Garner, B., Georgevich, A., Hodgson, A., Liu, L., Wallace, G., 1999. J. Biomed. Mater.
- Res. 44, 121–129.
- Gelmi, A., Cieslar-Pobuda, A., de Muinck, E., Los, M., Rafat, M., Jager, E.W., 2016. Adv. Healthc. Mater. 5, 1471–1480.
- GhavamiNejad, A., Park, C.H., Kim, C.S., 2016. Biomacromolecules 17, 1213–1223. Goding, J., Gilmour, A., Robles, U.A., Poole-Warren, L., Lovell, N., Martens, P., Green, R., 2017. Mrs Commun 7, 487–495.
- Goldin, M., Yerushalmi, J., Pfeffer, R., Shinnar, R., 1969. J. Fluid Mech. 38, 689–711. Green, R., Abidian, M.R., 2015. Adv. Mater. 27, 7620–7637.
- Green, R.A., Lovell, N.H., Poole-Warren, L.A., 2009. Biomaterials 30, 3637–3644.
- Green, R.A., Lovell, N.H., Poole-Warren, L.A., 2010. Acta Biomater. 6, 63–71.
- Green, R.A., Hassarati, R.T., Bouchinet, L., Lee, C.S., Cheong, G.L., Jin, F.Y., Dodds, C.W., Suaning, G.J., Poole-Warren, L.A., Lovell, N.H., 2012. Biomaterials 33, 5875–5886.
- Guan, Y.-S., Zhang, Z., Tang, Y., Yin, J., Ren, S., 2018. Adv. Mater. 30, 1706390. Guex, A.G., Puetzer, J.L., Armgarth, A., Littmann, E., Stavrinidou, E., Giannelis, E.P., Malliaras, G.G., Stevens, M.M., 2017. Acta Biomater. 62, 91–101.
- Guimard, N.K., Gomez, N., Schmidt, C.E., 2007. Prog. Polym. Sci. 32, 876-921.
- Gumus, A., Califano, J.P., Wan, A.M., Huynh, J., Reinhart-King, C.A., Malliaras, G.G., 2010. Soft Matter 6, 5138–5142.
- Guo, B., Ma, P.X., 2018. Biomacromolecules 19, 1764-1782.
- Guo, B., Glavas, L., Albertsson, A.-C., 2013. Prog. Polym. Sci. 38, 1263-1286.
- Guo, W., Zhang, X., Yu, X., Wang, S., Qiu, J., Tang, W., Li, L., Liu, H., Wang, Z.L., 2016. ACS Nano 10, 5086–5095.
- Hamedi, M.M., Campbell, V.E., Rothemund, P., Güder, F., Christodouleas, D.C., Bloch, J.-F., Whitesides, G.M., 2016. Adv. Funct. Mater. 26, 2446–2453.
- Hamid, S., Hayek, R., 2008. Eur. Spine J. 17, 1256-1269.
- Hammock, M.L., Chortos, A., Tee, B.C.-K., Tok, J.B.-H., Bao, Z., 2013. Adv. Mater. 25, 5997–6038.
- Heo, D.N., Song, S.-J., Kim, H.-J., Lee, Y.J., Ko, W.-K., Lee, S.J., Lee, D., Park, S.J., Zhang, L.G., Kang, J.Y., others, 2016. Acta Biomater. 39, 25–33.
- Hong, S.Y., Lee, Y.H., Park, H., Jin, S.W., Jeong, Y.R., Yun, J., You, I., Zi, G., Ha, J.S., 2016. Adv. Mater. 28, 930–935.
- Humpolicek, P., Kasparkova, V., Saha, P., Stejskal, J., 2012. Synth. Met. 162, 722–727.
 Inal, S., Rivnay, J., Suiu, A.-O., Malliaras, G.G., McCulloch, I., 2018. Acc. Chem. Res. 51, 1368–1376.
- Jahromi, M.A.M., Zangabad, P.S., Basri, S.M.M., Zangabad, K.S., Ghamarypour, A., Aref, A.R., Karimi, M., Hamblin, M.R., 2018. Adv. Drug Deliv. Rev. 123, 33–64.
- Jeon, H., Hong, S.K., Cho, S.J., Lim, G., 2018. Macromol. Mater. Eng. 303, 1700389.
 Jin, X., Jiang, H., Li, G., Fu, B., Bao, X., Wang, Z., Hu, Q., 2020. Chem. Eng. J. 124901.
 Joon, N.K., He, N., Ruzgas, T., Bobacka, J., Lisak, G., 2019. Anal. Chem. 91, 10524–10531.
- Kai, D., Prabhakaran, M.P., Jin, G., Ramakrishna, S., 2011. J. Biomed. Mater. Res. A 99, 376–385.
- Kang, J., Son, D., Wang, G.-J.N., Liu, Y., Lopez, J., Kim, Y., Oh, J.Y., Katsumata, T., Mun, J., Lee, Y., 2018. others. Adv. Mater. 30, 1706846.

- Kaur, G., Adhikari, R., Cass, P., Bown, M., Gunatillake, P., 2015. RSC Adv. 5, 37553–37567.
- Kenry, Liu, B., 2018. Biomacromolecules 19, 1783-1803.
- Khaldi, A., Maziz, A., Alici, G., Spinks, G.M., Jager, E.W., 2016. Sensor. Actuator. B Chem. 230, 818–824.
- Kim, R., Nam, Y., 2019. J. Neurosci. Methods 326, 108369.
- Kim, D.H., Richardson-Burns, S.M., Hendricks, J.L., Sequera, C., Martin, D.C., 2007. Adv. Funct. Mater. 17, 79–86.
- Kim, D.-M., Cho, S.J., Cho, C.-H., Kim, K.B., Kim, M.-Y., Shim, Y.-B., 2016. Biosens. Bioelectron. 79, 165–172.
- Kim, S., Jang, Y., Jang, L.K., Sunwoo, S.H., Kim, T., Cho, S.-W., Lee, J.Y., 2017. J. Mater. Chem. B 5, 4507–4513.
- Kim, S., Jang, L.K., Jang, M., Lee, S., Hardy, J.G., Lee, J.Y., 2018. ACS Appl. Mater. Interfaces 10, 33032–33042.
- Kim, Y., Kim, J., Lee, H., Park, C., Im, S., Kim, J.H., 2020. Macromol. Chem. Phys. 221, 1900465.
 Kleber, C., Bruns, M., Lienkamp, K., Rühe, J., Asplund, M., 2017. Acta Biomater. 58,
- 365–375. Klein, S.M., Melton, M.S., Grill, W.M., Nielsen, K.C., 2012. Reg. Anesth. Pain Med. 37,
- 383–392.
- Kline, R.J., McGehee, M.D., Kadnikova, E.N., Liu, J., Fréchet, J.M., Toney, M.F., 2005. Macromolecules 38, 3312–3319.
- Kotwal, A., Schmidt, C.E., 2001. Biomaterials 22, 1055-1064.
- Krack, P., Batir, A., Van Blercom, N., Chabardes, S., Fraix, V., Ardouin, C., Koudsie, A., Limousin, P.D., Benazzouz, A., LeBas, J.F., 2003. others. N. Engl. J. Med. 349, 1925–1934.
- Kurian, A.S., Souri, H., Mohan, V.B., Bhattacharyya, D., 2020. Sens. Actuators Phys. 112131.
- Larsson, K.C., Kjäll, P., Richter-Dahlfors, A., 2013. Biochim. Biophys. Acta BBA-Gen. Subj. 1830, 4334–4344.
- Lasia, A., 2002. Electrochemical impedance spectroscopy and its applications. In: Modern Aspects of Electrochemistry. Springer, pp. 143–248.
- Lee, J.Y., Bashur, C.A., Goldstein, A.S., Schmidt, C.E., 2009. Biomaterials 30, 4325–4335. Lee, S., Eom, T., Kim, M.-K., Yang, S.-G., Shim, B.S., 2019. Electrochim. Acta 313, 79–90.
- Lei, T., Guan, M., Liu, J., Lin, H.-C., Pfattner, R., Shaw, L., McGuire, A.F., Huang, T.-C., Shao, L., Cheng, K.-T., others, 2017. Proc. Natl. Acad. Sci. Unit. States Am. 114, 5107–5112.
- Leng, J., Lan, X., Liu, Y., Du, S., 2011. Prog. Mater. Sci. 56, 1077-1135.
- Li, Longchao, Ge, J., Ma, P.X., Guo, B., 2015a. RSC Adv. 5, 92490-92498.
- Li, Lanlan, Wang, Y., Pan, L., Shi, Ye, Cheng, W., Shi, Yi, Yu, G., 2015b. Nano Lett. 15, 1146–1151.
- Li, L., Pan, L., Ma, Z., Yan, K., Cheng, W., Shi, Y., Yu, G., 2018. Nano Lett. 18, 3322–3327.
- Li, G., Qiu, Z., Wang, Y., Hong, Y., Wan, Y., Zhang, J., Yang, J., Wu, Z., Hong, W., Guo, C. F., 2019. ACS Appl. Mater. Interfaces 11, 10373–10379.
- Lima, M.D., Li, N., De Andrade, M.J., Fang, S., Oh, J., Spinks, G.M., Kozlov, M.E., Haines, C.S., Suh, D., Foroughi, J., 2012. others. Science 338, 928–932.
- Lisak, G., Wagner, K., Barnsley, J.E., Veksha, A., Huff, G., Elliott, A.B., Wagner, P., Gordon, K.C., Bobacka, J., Wallace, G.G., 2018. others. RSC Adv. 8, 29505–29512.
- Liu, S., Wang, J., Zhang, D., Zhang, P., Ou, J., Liu, B., Yang, S., 2010. Appl. Surf. Sci. 256, 3427–3431.
- Liu, Y., Turner, A.P., Zhao, M., Mak, W.C., 2018. Biosens. Bioelectron. 100, 374-381.
- Liu, Y., Yin, P., Chen, J., Cui, B., Zhang, C., Wu, F., 2020. Int. J. Polym. Sci. 5659682. Löffler, S., Libberton, B., Richter-Dahlfors, A., 2015. Electronics 4, 879–908.
- Long, Y.-Z., Li, M.-M., Gu, C., Wan, M., Duvail, J.-L., Liu, Z., Fan, Z., 2011. Prog. Polym. Sci. 36, 1415–1442.
- Lu, M.-C., Ho, C.-Y., Hsu, S.-F., Lee, H.-C., Lin, J.-H., Yao, C.-H., Chen, Y.-S., 2008. Neurorehabilitation Neural Repair 22, 367–373.
- Lu, X., Zhang, Z., Li, H., Sun, X., Peng, H., 2014. J. Mater. Chem. A 2, 17272–17280.
- Lu, B., Yuk, H., Lin, S., Jian, N., Qu, K., Xu, J., Zhao, X., 2019a. Nat. Commun. 10, 1–10.
 Lu, Y., Liu, Z., Yan, H., Peng, Q., Wang, R., Barkey, M.E., Jeon, J.-W., Wujcik, E.K.,
 2019b. ACS Appl. Mater. Interfaces 11, 20453–20464.
- Luan, Y., Noh, J.-S., Kim, S.H., 2017. Mater. Chem. Phys. 190, 68-73.
- Lvovich, V.F., 2012. Impedance Spectroscopy: Applications to Electrochemical and Dielectric Phenomena.
- Ma, Y., Xin, L., Tan, H., Fan, M., Li, J., Jia, Y., Ling, Z., Chen, Y., Hu, X., 2017. Mater. Sci. Eng. C 81, 522–531.
- Macdonald, D.D., 2006. Electrochim. Acta 51, 1376–1388.
- Marroquin, J.B., Coleman, H.A., Tonta, M.A., Zhou, K., Winther-Jensen, B., Fallon, J., Duffy, N.W., Yan, E., Abdulwahid, A.A., Jasieniak, J.J., others, 2018. Adv. Funct. Mater. 28, 1700927.
- Martin, D.C., Malliaras, G.G., 2016. ChemElectroChem 3, 686-688.
- Mawad, D., Stewart, E., Officer, D.L., Romeo, T., Wagner, P., Wagner, K., Wallace, G.G., 2012. Adv. Funct. Mater. 22, 2692–2699.
- McGinness, J.E., 1972. Science 177, 896-897.
- McGinness, J., Corry, P., Proctor, P., 1974. Science 183, 853-855.
- Meijs, S., Alcaide, M., Sørensen, C., McDonald, M., Sørensen, S., Rechendorff, K., Gerhardt, A., Nesladek, M., Rijkhoff, N.J., Pennisi, C.P., 2016. J. Neural. Eng. 13, 056011.
- Meng, S., Rouabhia, M., Zhang, Z., 2013. Bioelectromagnetics 34, 189–199.
- Mihic, A., Cui, Z., Wu, J., Vlacic, G., Miyagi, Y., Li, S.-H., Lu, S., Sung, H.-W., Weisel, R. D., Li, R.-K., 2015. Circulation 132, 772–784.
- Miura, H., Fukuyama, Y., Sunda, T., Lin, B., Zhou, J., Takizawa, J., Ohmori, A., Kimura, M., 2014. Adv. Eng. Mater. 16, 550–555.
- Murbach, J.M., Currlin, S., Widener, A., Tong, Y., Chhatre, S., Subramanian, V., Martin, D.C., Johnson, B.N., Otto, K.J., 2018. MRS Commun 8, 1043–1049.

- Nezakati, T., Seifalian, A., Tan, A., Seifalian, A.M., 2018. Chem. Rev. 118, 6766–6843. Ning, C., Zhou, Z., Tan, G., Zhu, Y., Mao, C., 2018. Prog. Polym. Sci. 81, 144–162.
- Oh, J.Y., Kim, S., Baik, H.-K., Jeong, U., 2016. Adv. Mater. 28, 4455–4461.
- Okuzaki, H., Kunugi, T., 1998. J. Polym. Sci., Part B: Polym. Phys. 36, 1591–1594. Okuzaki, H., Suzuki, H., Ito, T., 2009. J. Phys. Chem. B 113, 11378–11383.
- Okuzaki, H., Kuwabara, T., Funasaka, K., Saido, T., 2013. Adv. Funct. Mater. 23, 4400–4407.
- Opie, N.L., John, S.E., Rind, G.S., Ronayne, S.M., Grayden, D.B., Burkitt, A.N., May, C.N., O'Brien, T.J., Oxley, T.J., 2016. J. Neural. Eng. 13, 046020.
- Osak, W., Tkacz, K., Czternastek, H., S\lAwiński, J., 1989. Biopolym. Orig. Res. Biomol. 28, 1885–1890.
- Owen, A.M., 2004. Neuroscientist 10, 525-537.
- Ozawa, H., Abe, E., Shibasaki, Y., Fukuhara, T., Suda, T., 1989. J. Cell. Physiol. 138, 477–483.
- Pal, R.K., Pradhan, S., Narayanan, L., Yadavalli, V.K., 2018. Sensor. Actuator. B Chem. 259, 498–504.
- Park, J.S., Park, K., Moon, H.T., Woo, D.G., Yang, H.N., Park, K.-H., 2009. Langmuir 25, 451–457.
- Park, S., Guo, Y., Jia, X., Choe, H.K., Grena, B., Kang, J., Park, J., Lu, C., Canales, A., Chen, R., 2017. others. Nat. Neurosci. 20, 612–619.
- Park, J.-K., Kang, T.-G., Kim, B.-H., Lee, H.-J., Choi, H.H., Yook, J.-G., 2018. Sci. Rep. 8, 1–8.
- Patil, A.C., Thakor, N.V., 2016. Med. Biol. Eng. Comput. 54, 23-44.
- Plesse, C., Vidal, F., Teyssié, D., Chevrot, C., 2010. Chem. Commun. 46, 2910–2912.
- Powell, M.R., Rosenberg, B., 1970. Biopolym. Orig. Res. Biomol. 9, 1403–1406. Prabhakaran, M.P., Venugopal, J.R., Ramakrishna, S., 2009. Biomaterials 30, 4996–5003.
- Qi, D., Liu, Z., Liu, Y., Jiang, Y., Leow, W.R., Pal, M., Pan, S., Yang, H., Wang, Y., Zhang, X., 2017. others. Adv. Mater. 29, 1702800.
- Qiang, Y., Seo, K.J., Zhao, X., Artoni, P., Golshan, N.H., Culaclii, S., Wang, P.-M., Liu, W., Ziemer, K.S., Fagiolini, M., 2017. others. Adv. Funct. Mater. 27, 1704117.
- Qu, J., Zhao, X., Liang, Y., Xu, Y., Ma, P.X., Guo, B., 2019. Chem. Eng. J. 362, 548–560.
- Quigley, A.F., Razal, J.M., Thompson, B.C., Moulton, S.E., Kita, M., Kennedy, E.L., Clark, G.M., Wallace, G.G., Kapsa, R.M., 2009. Adv. Mater. 21, 4393–4397.
- Rahimi, R., Ochoa, M., Parupudi, T., Zhao, X., Yazdi, I.K., Dokmeci, M.R., Tamayol, A., Khademhosseini, A., Ziaie, B., 2016. Sensor. Actuator. B Chem. 229, 609–617
- Rahimi, R., Ochoa, M., Tamayol, A., Khalili, S., Khademhosseini, A., Ziaie, B., 2017. ACS Appl. Mater. Interfaces 9, 9015–9023.
- Rivers, T.J., Hudson, T.W., Schmidt, C.E., 2002. Adv. Funct. Mater. 12, 33–37.
- Ryaby, J.T., 1998. Clin. Orthop. Relat. Res. 355, S205-S215.
- Ryu, M., Yang, J.H., Ahn, Y., Sim, M., Lee, K.H., Kim, K., Lee, T., Yoo, S.-J., Kim, S.Y., Moon, C., others, 2017. ACS Appl. Mater. Interfaces 9, 10577–10586.
- Schläpfer, T., Kayser, S., 2014. Klin. Neurophysiol. 45, 113–117.
- Schoenen, J., Di Clemente, L., Vandenheede, M., Fumal, A., De Pasqua, V., Mouchamps, M., Remacle, J.-M., de Noordhout, A.M., 2005. Brain 128, 940–947.
- Sessolo, M., Khodagholy, D., Rivnay, J., Maddalena, F., Gleyzes, M., Steidl, E., Buisson, B., Malliaras, G.G., 2013. Adv. Mater. 25, 2135–2139.
- Shahini, A., Yazdimamaghani, M., Walker, K.J., Eastman, M.A., Hatami-Marbini, H., Smith, B.J., Ricci, J.L., Madihally, S.V., Vashaee, D., Tayebi, L., 2014. Int. J. Nanomed. 9, 167.
- Shang, L., Huang, Z., Pu, X., Yin, G., Chen, X., 2019. ACS Biomater. Sci. Eng. 5, 1268–1278.
- Simaite, A., Tondu, B., Soueres, P., Bergaud, C., 2015. ACS Appl. Mater. Interfaces 7, 19966–19977.
- Sinha, S., Bhadra, S., Khastgir, D., 2009. J. Appl. Polym. Sci. 112, 3135–3140.
- Sirringhaus, H., Brown, P., Friend, R., Nielsen, M.M., Bechgaard, K., Langeveld-Voss, B., Spiering, A., Janssen, R.A., Meijer, E., Herwig, P., 1999. Nature 401, 685–688 others.
- Spearman, B.S., Hodge, A.J., Porter, J.L., Hardy, J.G., Davis, Z.D., Xu, T., Zhang, X., Schmidt, C.E., Hamilton, M.C., Lipke, E.A., 2015. Acta Biomater. 28, 109–120.
- Staples, N.A., Goding, J.A., Gilmour, A.D., Aristovich, K.Y., Byrnes-Preston, P., Holder, D. S., Morley, J.W., Lovell, N.H., Chew, D.J., Green, R.A., 2018. Front. Neurosci. 11, 748.
- Strakosas, X., Wei, B., Martin, D.C., Owens, R.M., 2016. J. Mater. Chem. B 4, 4952–4968. Talikowska, M., Fu, X., Lisak, G., 2019. Biosens. Bioelectron. 135, 50–63.
- Taroni, P.J., Santagiuliana, G., Wan, K., Calado, P., Qiu, M., Zhang, H., Pugno, N.M., Palma, M., Stingelin-Stutzman, N., Heeney, M., 2018. others. Adv. Funct. Mater. 28, 1704285

- Teo, M.Y., Kim, N., Kee, S., Kim, B.S., Kim, G., Hong, S., Jung, S., Lee, K., 2017. ACS Appl. Mater. Interfaces 9, 819–826.
- Theodore, W.H., Fisher, R.S., 2004. Lancet Neurol. 3, 111-118.
- Trung, T.Q., Ramasundaram, S., Hwang, B.-U., Lee, N.-E., 2016. Adv. Mater. 28, 394–394.
- Vivó, M., Puigdemasa, A., Casals, L., Asensio, E., Udina, E., Navarro, X., 2008. Exp. Neurol. 211, 180–193.
- Vomero, M., Castagnola, E., Ciarpella, F., Maggiolini, E., Goshi, N., Zucchini, E., Carli, S., Fadiga, L., Kassegne, S., Ricci, D., 2017. Sci. Rep. 7, 1–14.
- Vunjak-Novakovic, G., Tandon, N., Godier, A., Maidhof, R., Marsano, A., Martens, T.P., Radisic, M., 2010. Tissue Eng. B Rev. 16, 169–187.
- Vuorinen, T., Niittynen, J., Kankkunen, T., Kraft, T.M., Mäntysalo, M., 2016. Sci. Rep. 6,
- Wang, B., Facchetti, A., 2019. Adv. Mater. 31, 1901408.
- Wang, Z., Roberge, C., Dao, L.H., Wan, Y., Shi, G., Rouabhia, M., Guidoin, R., Zhang, Z., 2004. J. Biomed. Mater. Res. Part Off. J. Soc. Biomater. Jpn. Soc. Biomater. Aust. Soc. Biomater. Korean Soc. Biomater. 70, 28–38.
- Wang, Z., Clark, C.C., Brighton, C.T., 2006. JBJS 88, 1053-1065.
- Wang, B., Qin, D., Liang, G., Gu, A., Liu, L., Yuan, L., 2013. J. Phys. Chem. C 117, 15487–15495.
- Wang, D., Lu, C., Zhao, J., Han, S., Wu, M., Chen, W., 2017a. RSC Adv. 7, 31264–31271.
 Wang, Y., Zhu, C., Pfattner, R., Yan, H., Jin, L., Chen, S., Molina-Lopez, F., Lissel, F.,
 Liu, J., Rabiah, N.I., 2017b. others. Sci. Adv. 3, e1602076.
- Wang, L., Wu, Y., Hu, T., Guo, B., Ma, P.X., 2017c. Acta Biomater. 59, 68-81.
- Wang, S., Guan, S., Zhu, Z., Li, W., Liu, T., Ma, X., 2017d. Mater. Sci. Eng. C 71, 308–316.
 Wang, S., Sun, C., Guan, S., Li, W., Xu, J., Ge, D., Zhuang, M., Liu, T., Ma, X., 2017e.
 J. Mater. Chem. B 5, 4774–4788.
- Wang, T., Zhang, Y., Liu, Q., Cheng, W., Wang, X., Pan, L., Xu, B., Xu, H., 2018. Adv. Funct. Mater. 28, 1705551.
- Wang, L.-C., Wang, M.-H., Ge, C.-F., Ji, B.-W., Guo, Z.-J., Wang, X.-L., Yang, B., Li, C.-Y., Liu, J.-Q., 2019. Biosens. Bioelectron. 145, 111661.
- Wang, Z., Cong, Y., Fu, J., 2020. J. Mater. Chem. B 8, 3437-3459.
- Wen, Z., Yang, Y., Sun, N., Li, G., Liu, Y., Chen, C., Shi, J., Xie, L., Jiang, H., Bao, D., others, 2018. Adv. Funct. Mater. 28, 1803684.
- Williams, R., Doherty, P., 1994. J. Mater. Sci. Mater. Med. 5, 429–433.
- Woeppel, K., Yang, Q., Cui, X.T., 2017. Curr. Opin. Biomed. Eng. 4, 21–31.
- Wong, J.Y., Langer, R., Ingber, D.E., 1994. Proc. Natl. Acad. Sci. Unit. States Am. 91, 3201–3204.
- Xia, Y., Lu, X., Zhu, H., 2013. Compos. Sci. Technol. 77, 37-41.
- Xie, Y., Zheng, Y., Fan, J., Wang, Y., Yue, L., Zhang, N., 2018. ACS Appl. Mater. Interfaces 10, 22692–22702.
- Xu, D., Fan, L., Gao, L., Xiong, Y., Wang, Y., Ye, Q., Yu, A., Dai, H., Yin, Y., Cai, J., others, 2016. ACS Appl. Mater. Interfaces 8, 17090–17097.
- Yazdimamaghani, M., Razavi, M., Mozafari, M., Vashaee, D., Kotturi, H., Tayebi, L., 2015. J. Mater. Sci. Mater. Med. 26. 274.
- Zare, E.N., Makvandi, P., Ashtari, B., Rossi, F., Motahari, A., Perale, G., 2019. J. Med. Chem. 63, 1–22.
- Zhang, Z., Rouabhia, M., Wang, Z., Roberge, C., Shi, G., Roche, P., Li, J., Dao, L.H., 2007. Artif. Organs 31, 13–22.
- Zhang, X., Qi, H., Wang, S., Feng, L., Ji, Y., Tao, L., Li, S., Wei, Y., 2012. Toxicol. Res. 1, 201–205.
- Zhao, Y., Liang, Y., Ding, S., Zhang, K., Mao, H., Yang, Y., 2020. Biomaterials, 120164. Zhou, H., Cheng, X., Rao, L., Li, T., Duan, Y., 2013. 9, 6439-6449.
- Zhou, J., Mulle, M., Zhang, Y., Xu, X., Li, E.Q., Han, F., Thoroddsen, S.T., Lubineau, G., 2016. J. Mater. Chem. C 4, 1238–1249.
- Zhou, X., Wang, H., Zhang, J., Li, X., Wu, Y., Wei, Y., Ji, S., Kong, D., Zhao, Q., 2017.
 Acta Biomater. 54, 128–137.
 Zhou, L., Fan, L., Yi, X., Zhou, Z., Liu, C., Fu, R., Dai, C., Wang, Z., Chen, X., Yu, P., 2018.
- ACS Nano 12, 10957–10967 others.
 Zhu, B., Wang, H., Leow, W.R., Cai, Y., Loh, X.J., Han, M.-Y., Chen, X., 2016. Adv. Mater.
- 28, 4250–4265.
- Zia, S., Mozafari, M., Natasha, G., Tan, A., Cui, Z., Seifalian, A.M., 2016. Crit. Rev. Biotechnol. 36, 705–715.
- Zou, Y., Qin, J., Huang, Z., Yin, G., Pu, X., He, D., 2016. ACS Appl. Mater. Interfaces 8, 12576–12582.